Mon. Not. R. Astron. Soc. **293,** 124–144 (1998)

A statistical analysis of the galaxy populations of distant luminous X-ray clusters

Ian Smail,[1] Alastair C. Edge,[2] Richard S. Ellis[2] and Roger D. Blandford[3]

[1]*Department of Physics, University of Durham, Durham DH1 3LE*
[2]*Institute of Astronomy, Madingley Road, Cambridge CB3 0HA*
[3]*Theoretical Astrophysics, Caltech 130-33, Pasadena CA 91125, USA*

Accepted 1997 August 27. Received 1997 August 27; in original form 1997 February 27

ABSTRACT

We present a deep, multicolour (*UBI*) CCD survey using the Palomar 5-m telescope of a sample of high X-ray luminosity, distant clusters selected from the *ROSAT* All-Sky Survey. The 10 clusters lie in the redshift range $z = 0.22–0.28$, an era in which evolutionary effects have been reported in the properties of cluster galaxy populations. Our clusters thus provide a well-defined sample of the most massive systems at these redshifts with which to quantify the extent and variability of these evolutionary effects. The relatively low redshifts of these clusters also means that simple connections can be made between the galaxy populations of these clusters and their immediate descendents, local rich clusters. Moreover, by concentrating on a narrow redshift range, we can take advantage of the homogeneity of our cluster sample to combine the galaxy catalogues from all the clusters to analyse statistically the bulk properties of their populations. We present an analysis of the cluster galaxy populations using our multicolour data to probe the distribution, luminosities and star formation histories of galaxies in these regions. Our aim is to chart the characteristics of the galaxy populations of massive intermediate redshift clusters and to combine these into a wider scheme for galaxy evolution in high-density environments.

The core regions of clusters in our sample contain only a small proportion of star-forming galaxies, and they therefore do not exhibit a classical 'Butcher–Oemler' effect. Focusing on the redder cluster galaxies, we find that their integrated luminosity is well correlated with the X-ray temperatures of the clusters, and hence with cluster mass. Furthermore, the typical rest frame UV–optical colours of the luminous elliptical sequences in the clusters exhibit a remarkably small cluster-to-cluster scatter, $\lesssim 2$ per cent, indicating that these galaxies are highly homogeneous between cluster environments. However, at fainter magnitudes we observe a marked increase in the range of mid-UV colours of galaxies possessing strong 4000-Å breaks, as determined from photometry in $\sim 7.5\,h^{-1}$ kpc diameter apertures. In the light of the apparent decline in the population of S0 galaxies seen in distant, $z \gtrsim 0.4$, clusters, and in view of the luminosities and colours of this population, we propose that they may be the progenitors of the dominant S0 population of local rich clusters, caught in the final stage before they become completely quiescent. Further studies of this population will prove a necessary link with which to connect the evolution observed in cluster populations at high redshift with the nature of the final remnants locally. Observations in the rest frame UV will be important in these studies owing to the relative ease of detecting the signature of previous activity in this spectral region.

Key words: galaxies: clusters: general – galaxies: luminosity function, mass function – galaxies: photometry – cosmology: observations – X-rays: general.

1 INTRODUCTION

The study of galaxies in rich clusters at earlier epochs has long been seen as one of the best routes to understanding the role of environment in the evolution of galaxy populations, as well as more general issues of galaxy formation. For this reason a number of groups have studied the photometric and spectroscopic properties of galaxies in distant clusters (e.g. Butcher & Oemler 1978, 1984; Couch & Sharples 1987; Dressler & Gunn 1992; Aragón-Salamanca et al. 1993; Barger et al. 1996). One of the most interesting conclusions of these studies has been the realization that the luminous elliptical population which dominates local cluster cores (Dressler 1980) has been in place for a considerable time, at least prior to $z \sim 0.6$ (Ellis et al. 1997; Smail et al. 1997a) and possibly earlier than $z \sim 1$ (Faber et al. 1997; Stanford, Eisenhardt & Dickinson 1998; Lubin et al., in preparation). All indications are that this population has undergone only passive evolution in the recent past (Van Dokkum & Franx 1996; Ellis et al. 1997; Stanford et al. 1998; Barger et al. 1998). In contrast to the relative stability of the elliptical population, the other major component of the local cluster population, S0 galaxies, are claimed to be relatively rare in distant clusters (Dressler et al. 1997). The recent formation or transformation of this population and the nature of the process responsible for it are therefore of considerable interest for understanding the extent of environmental influences on galaxy morphology.

The most dramatic evidence for evolutionary change in the cluster population, however, is seen in the blue galaxy populations of these regions (Butcher & Oemler 1978, 1984; Couch & Sharples 1987; Dressler & Gunn 1992). Butcher & Oemler's extensive study of a heterogeneous sample of distant clusters indicated a substantial increase in the blue populations of rich clusters at $z \gtrsim 0.2$. Recent *Hubble Space Telescope* (*HST*) work on these systems has shown that these objects are mainly disc galaxies, some of which are interacting (Couch et al. 1994, 1998 and in preparation; Dressler et al. 1994; Smail et al. 1997a). The absence of this population from similar environments in local clusters may connect with the large present-day populations of S0s in these regions. Mechanisms proposed for removing or transforming these star-forming galaxies from the centres of clusters include ram-pressure stripping from the intracluster medium (ICM) (Gunn & Gott 1972), tidal effects due to the cluster potential (Byrd & Valtonen 1990) and interactions with other cluster galaxies (Moore et al. 1996). To date, however, few well-defined samples of distant clusters have been available with which to test the different correlations predicted by these mechanisms (cf. the L_X–f_{sp} relation shown by Edge & Stewart 1991, or the mass–f_{sp} relation of Smail et al. 1997b). Such samples are also necessary to link the observations at different redshifts, by providing an understanding of the parallel evolution of the structures which the galaxies inhabit.

Here we describe a statistical analysis of the galaxy populations in a large, well-defined sample of 10 distant clusters at $z = 0.2$–0.3, selected on the basis of their X-ray emission. Our sample focuses on the systems with the highest X-ray luminosity (L_X); from this we hope to understand the variation in the properties of massive clusters across a relatively narrow mass range, and the effects this has had on the galaxy populations in such regions. In particular, we will concentrate on the variation in the star formation histories of the luminous elliptical populations between clusters, as determined from their UV–optical colours. This is a technique previously only applied to small samples of two to three clusters (Bower, Lucey & Ellis 1992, hereafter BLE; Ellis et al. 1997); here we can compare a homogeneous sample of 10 clusters imaged in identical conditions to robustly determine the cluster-to-cluster scatter. In particular, we illustrate how our combination of *UBI* imaging is particularly useful for searching for the signature of recent star formation in more quiescent systems. We show the advantages of working in the rest frame mid-UV for detecting even small traces of past activity in certain populations (Dorman, O'Connell & Rood 1995). We also study the blue populations of these clusters, using the large positive *K*-correction in *U* for these galaxies to identify them relative to the passive cluster galaxies. We focus on the varying proportion of this blue, star-forming population in the clusters and the dependence of this component on the global properties of the clusters. Our final aim is to understand the relationships between the various galactic components of the clusters within the framework of a simple model for their growth and evolution.

This study is particularly timely given recent theoretical work in this area (Bower 1991; Baugh, Cole & Frank 1996a, 1996b; Moore et al. 1996). The integration of spectral evolution models with simple dynamical models for structure formation, allows us for the first time to begin to compare theory and observations in this field (e.g. Baugh et al. 1996a). Detailed *N*-body simulations are also now well placed to follow the dynamical evolution of galaxies within cluster potentials (e.g. Moore et al. 1996; Moore, Lake & Katz 1998). These types of quantitative comparisons are the ones that will benefit from the well-defined cluster sample we use. This paper is thus part of an on-going programme to map out the properties of the galaxy populations in the most massive collapsed structures in the universe as a function of epoch out to $z \sim 0.5$. The data described here deal with the statistical analysis of the galaxy populations in luminous X-ray clusters in the range $0.2 \leq z \leq 0.3$. A similar study using very-wide-field CCD imaging and spectroscopy of a sample of luminous X-ray clusters at $0.07 \leq z \leq 0.15$ is underway (O'Hely et al., in preparation); this will provide a continuous coverage of the evolution of the most massive clusters and their galaxy populations from $z \sim 0$–0.3.

Previous work linking the galaxy population of distant clusters with their global characteristics has concentrated on the blue, star-forming or 'Butcher–Oemler' galaxies in distant clusters (Lea & Henry 1988) and has found little evidence relating their characteristics to the X-ray properties of the clusters (although see Wang & Ulmer 1997). Nevertheless, there is still much discussion of the role of the X-ray-emitting gas of a cluster in affecting the properties of its galaxy populations. We note, however, that the necessity for such processes to power the Butcher–Oemler (BO) effect is diminishing. It is no longer apparent that the star formation rates seen in the distant BO galaxies are in any way extreme given the characteristics of the surrounding field population (Couch et al., in preparation), and the only class of objects thought to be uniquely associated with the BO effect in the distant clusters, the post-starburst galaxies

Table 1. The log of observations and our cluster sample. We list the field identifications, position and cluster redshift, as well as the total integration times and seeing of the *UBI* images of the clusters. We then give the 80 per cent completeness of the *I*-band catalogues from comparison with deeper field counts and the estimated reddening in these directions. The final three columns give the angular scale at the cluster redshift for our adopted cosmology (in units of h^{-1} kpc arcsec^{-1}), the total area covered by our images in each cluster in arcmin^2, the X-ray luminosity of the clusters in the 0.2–2.4 keV band in units of $h^{-1}\,10^{44}$ erg s^{-1} and the X-ray temperatures in keV from Mushotzky & Scharf (1997) where available.

Cluster	RA	Dec	z	T_{exp} (ks)			FWHM ($''$)			I	$E(B-V)$	Scale	Area	L_X	T_X
	(J2000)	(J2000)		U	B	I	U	B	I	(80%)					
A1682	13 06 52.4	+46 33 05	0.226	3.0	0.6	0.5	1.19	1.47	0.87	22.5	0.03	2.30	92.55	2.79	...
A1704	13 14 24.5	+64 34 30	0.220	3.6	0.5	0.5	1.37	1.63	1.31	22.5	0.04	2.26	89.30	1.69	4.5
A1758	13 32 44.0	+50 32 33	0.280	3.0	0.5	0.5	1.17	1.27	1.05	22.5	0.02	2.64	86.46	2.81	10.2
A1763	13 35 18.5	+40 59 46	0.228	3.0	0.5	0.5	1.22	1.41	1.07	22.5	0.02	2.31	90.96	3.62	9.0
A1835	14 01 02.2	+02 52 43	0.253	3.0	0.5	1.0	1.43	1.72	1.14	22.5	0.05	2.47	82.74	9.59	8.2
Zw7160	14 57 14.9	+22 20 35	0.256	3.0	0.6	1.0	1.23	1.67	1.10	23.0	0.07	2.49	84.84	3.37	5.5
A2146	15 56 11.5	+66 21 30	0.234	3.0	0.5	0.5	1.31	1.24	1.15	23.0	0.06	2.35	92.55	2.15	...
A2219	16 40 20.5	+46 42 29	0.228	3.7	1.0	0.5	1.54	1.25	1.10	22.5	0.04	2.31	92.60	4.95	11.8
A2261	17 22 26.8	+32 07 59	0.225	3.0	0.5	0.5	1.35	1.29	1.04	22.5	0.07	2.29	93.01	4.51	...
A2390	21 53 36.8	+17 41 46	0.233	3.0	0.5	0.9	1.43	1.37	1.13	22.5	0.14	2.34	92.69	5.31	8.9
Field	00 53 23.2	+12 33 58	...	28.0	1.0	1.0	1.10	1.20	1.10	23.0	0.00	...	81.00	...	...

(PSG) or 'E + A', have recently been discovered in the local field (Zabludoff et al. 1996). Hence, although our study focuses on a sample of luminous X-ray clusters, our emphasis is on the use of the X-ray properties of the clusters to provide a well-defined sample of massive clusters and also to give some insight into their dynamical states, rather than simply to test possible interactions between the galaxy populations and the cluster X-ray gas.

We briefly describe the structure of this paper. Section 2 details the observations and the reduction and analysis thereof. In Section 3 we catalogue the galaxy populations in our clusters before describing our analysis of these catalogues in order to study the properties of the cluster populations, both the evolved red spheroidal systems and the star-forming galaxies associated with the clusters. Finally, in Section 4 we discuss our results and give our main conclusions.

2 OBSERVATIONS AND ANALYSIS

The cluster sample we elected to use for this study is ideally suited for investigating the properties of the galaxy populations in the most massive collapsed structures at $z \sim 0.2$. The sample contains a total of 24 of the most luminous X-ray clusters in the redshift range $0.2 < z < 0.3$ selected from the northern section of the *ROSAT* All-Sky Survey, as given in an early compilation of the Brightest Cluster Sample of Ebeling et al. (1996). These clusters all have X-ray luminosities in excess of $L_X(0.1\text{–}2.4) \geq 2 \times 10^{44}\,h^{-1}$ erg s^{-1},[1] indicating that their typical masses are: $M \geq M_{\rm Coma}$ and they thus represent some of the most massive collapsed structures known. This is also supported by the richnesses of these systems as demonstrated by our analysis below. The X-ray luminosities derived from *ROSAT* HRI imaging are presented in Table 1 and are discussed in more detail in Edge et al. (in preparation). The sample has also been subjected to extensive X-ray observations, providing deep, high-resolution X-ray images of all the clusters and X-ray spectroscopy of all but one. These X-ray images show that the majority of the clusters have relatively simple morphologies, the most obvious exception being the bimodal cluster A1758 (Fig. 1) which exhibits a highly elongated X-ray morphology. Most importantly, for the simple comparison of galaxy populations, the whole sample spans only a modest range in redshift, minimizing differential *K*-corrections. We have obtained deep and wide-field, multicolour imaging of a subsample of 10 of these clusters (those with right ascensions in the range 13–22^h) for the analysis here. One particular feature of this project has been our use of a blue-sensitive CCD, allowing us to acquire deep *U*-band (rest frame $\sim$2900 Å in the mid-UV) images of the clusters. The *U* filter used for this study is a copy of Bessell's *U* (Bessell 1990) kindly made available to us by Dr J. Schombert. Our standard Johnson *B* and Cousins *I* exposures provide complimentary information on the cluster galaxies at rest frame wavelengths around $\sim$3600 and $\sim$6600 Å, very close to *U* and *R* respectively.

The catalogue of candidate gravitationally lensed features from our survey is given in Edge et al. (1988), while the galaxy populations in some of the individual clusters are briefly discussed in Smail et al. (1995b) and Allen et al. (1996). X-ray imaging of the clusters in this sample is presented in Edge et al. (in preparation).

2.1 Observations and reduction

The data discussed here comprise *UBI* imaging of all 10 clusters. These data were acquired using the COSMIC

[1]We take $h = H_0/100$ km s^{-1} Mpc^{-1} and $q_0 = 0.5$ unless otherwise stated.

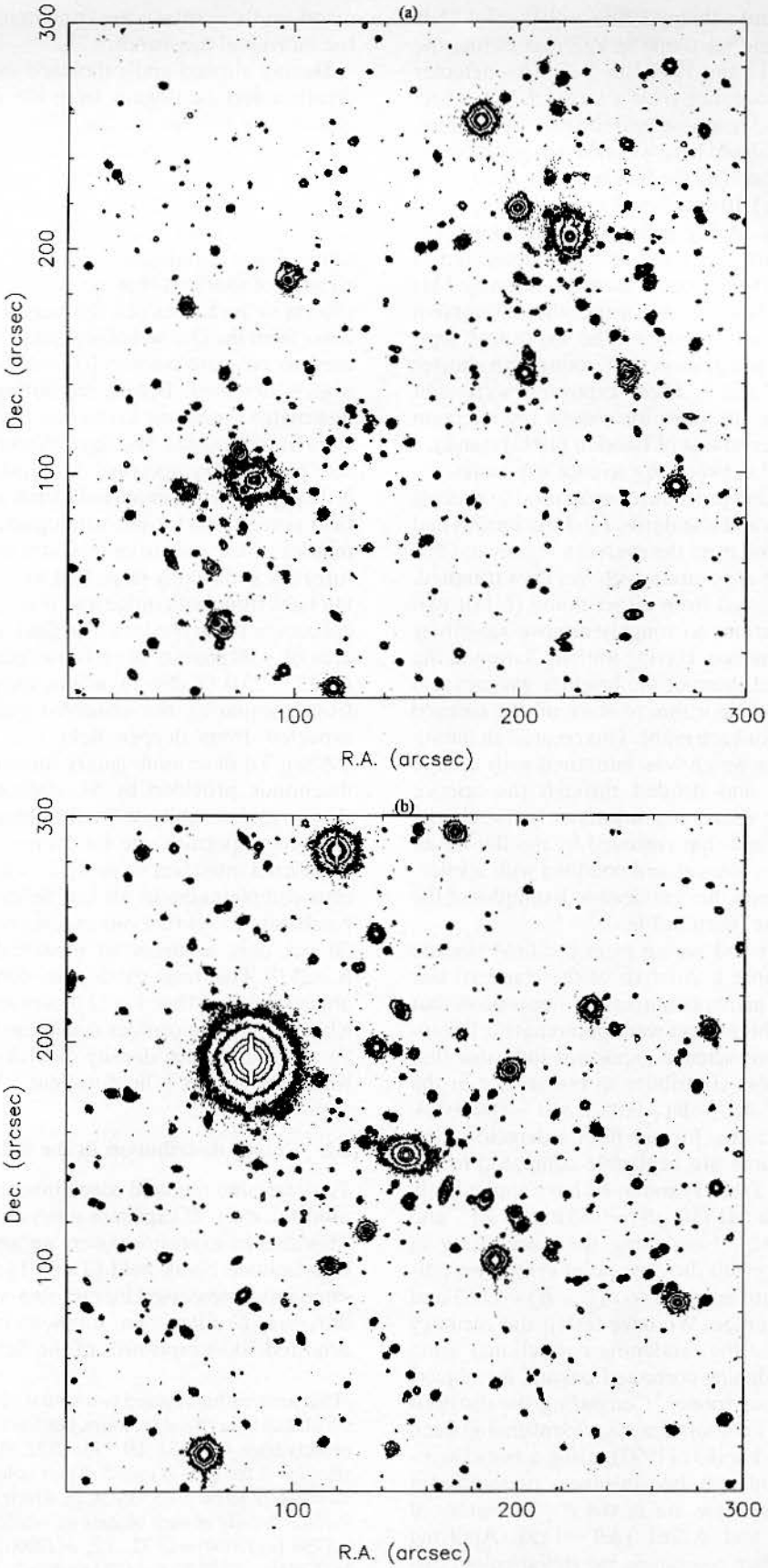

Figure 1. *I*-band images of the central 5×5 arcmin regions of two of the clusters in our sample (a) A1758 ($z = 0.280$) and (b) A1763 ($z = 0.228$). Note the two luminous galaxies at the upper-right and lower-left of the field in A1758; these are the central galaxies of the two prominent components of this bimodal cluster. The lowest contour corresponds to $\mu_I = 23.5$ mag arcsec^{-2}, equivalent to 3.5σ pixel^{-1}.

imaging spectrograph and a thinned 2048 × 2048 pixel TEK detector on the 5-m Hale telescope at Palomar during the nights of 1994 June 9–12 and 1994 July 5–7. This detector provides 0.284 arcsec sampling over a large, 9.7 × 9.7 arcmin, field with very good response into the near-ultraviolet. The bulk of the data analysed here was taken in good conditions during the June run. The median seeing in the I-band during these nights was 1.10 arcsec and the nights appeared stable and photometric. A log giving the field identifications, positions, exposure times and seeing is presented in Table 1. The reddening values come from the estimated H I column densities in these fields, using the conversion $E(B-V)=N(\mathrm{H\,I})/(4.8\times10^{21}\ \mathrm{cm}^{-2})$. The exposures typically comprise a 3000-s integration in U, along with shorter 500-s integrations in B and I. These exposures were split into ~2–4 subexposures to allow for cosmic ray rejection during processing. Observations of Landolt (1992) standard fields were interspersed between the science exposures.

Standard IRAF reduction procedures were used to process both the science frames and standards. First the images had their bias levels calculated from the overscan region and this was subtracted from the exposure, which was then trimmed. Flat-fields were constructed from either dome (U) or twilight (B and I) observations to roughly remove sensitivity gradients across the detector. Having initially flattened the frames, we then cleaned them of the brighter galaxies and stars and used a median algorithm to stack all the cleaned frames in a given filter for each night. This created an illumination correction frame which was smoothed with a large box filter, normalized and divided through the science frames to remove any remaining mismatch between the 'true' sky illumination and that removed by the flat-fields. These frames were then aligned and coadded with a rejection algorithm to eliminate the cosmic rays. Examples of the final reduced images are given in Fig. 1.

Total exposure times and seeing from the final stacked images are listed in Table 1. Analysis of the standard star exposures through the nights confirms our impression that all the nights used for this project were photometric. Photometric calibration of our science exposures indicates that average zero-point errors contribute to the scatter in the colours at the level of $\delta(U-B)=0.052$, $\delta(B-I)=0.024$. Analysis of the colour terms for our filter + detector combinations shows that these are negligible compared to the reddening corrections (Table 1) and so we have applied only the latter correction [$E(U-B)=0.85E(B-V)$ and $E(B-I)=2.45E(B-V)$]. Combining the uncertainty in the reddenings (±0.01) with the zero-point errors, we estimate that our colours are accurate to $\delta(U-B)=0.053$ and $\delta(B-I)=0.034$, on average. We have tested the accuracy of our photometry (and the reddening corrections) using the distribution of reddening-corrected colours for objects identified as stars on our frames. Comparing the distribution in $(U-B)$–$(B-I)$ colours for stars identified in each cluster to that given in Landolt (1992), using a two-dimensional K–S test we find only two instances of significant (>99 per cent) offsets; these are in the B photometry of A2390 ($\Delta B=-0.14$) and A2261 ($\Delta B=0.12$). Applying these corrections and then combining the stellar colour distributions for 314 stars in the 10 clusters we determine limits on the maximum offsets in our mean colours of $\Delta(U-B)=0.02\pm0.04$ and $\Delta(B-I)=-0.04\pm0.05$. The errors on these offsets are consistent with those claimed for the individual passbands.[2]

Having aligned and calibrated our *UBI* images we now create object catalogues from the I-band images of each cluster. For this we use the SExtractor package (Bertin & Arnouts 1996) to detect and analyse galaxies on the I frames. We adopt a detection criterion of 10 contiguous pixels, each 1σ (of the pixel-to-pixel noise) above the local background, after convolution with a 3 × 3 pixel top-hat filter. These catalogues are then visually inspected and cleaned of spurious objects (e.g. diffraction spikes and noise objects in the haloes of a few very bright stars). The coordinates from the cleaned object catalogues so created are then used to measure colours [$(U-B)$ and $(B-I)$] for all the objects detected. Before measuring colours, however, we first match the seeing in the *UBI* frames from the profiles of stars in the images. We have chosen to use a fixed angular size photometry aperture 3.0 arcsec in diameter (6.8–7.9 h^{-1} kpc), rather than a fixed metric aperture, to simplify the field corrections for our catalogues. We discuss the uncertainties which arise from this later in the paper. These apertures are sufficiently large that we should detect the bulk of the light from both bulge and disc components of luminous galaxies in these clusters. The final frames typically cover an area of ~90 arcmin^2 to an 80 per cent completeness limit of $I=22.5$–23.0 (Table 1), where these values are estimated from comparing the observed galaxy counts with those expected from deeper field observations (Smail et al. 1995a). To determine galaxy luminosities we use the BEST magnitude provided by SExtractor, which is based on a 'Kron-type' magnitude for brighter galaxies, with a fixed minimum aperture size for fainter objects. In our analysis we restrict ourselves to an $I\leq22$ sample to ensure $\gtrsim$95 per cent completeness in all our fields. Analysis of the other passbands shows that our exposures provide photometry to 20 per cent accuracy to median limits of $U=25.1$ and $B=25.9$. The final catalogues contain a total of 11 211 objects brighter than $I=22.0$ over an area of 898 arcmin^2, of which 1138 have profiles consistent with being stars, giving an average surface density of 11.2 ± 2.3 galaxies arcmin^{-2}, where the scatter is field-to-field.

2.2 Colour distribution in the field

To determine the field correction for our cluster frames we used the deep U exposure analysed by Hogg et al. (1997). This 28.0-ks exposure covers an area of 81.0 arcmin^2 in a high-latitude blank field (Table 1) and was taken with the same instrument used for our observations, although using a different U filter. To supplement this observation we acquired 500-s exposures of the field in B and I during the

[2]This analysis highlighted two stellar objects in our $I<20$ sample which had blue $(B-I)$ colours, but were very red in $(U-B)$. These objects have $I=18.33$, $(B-I)=2.52$, $(U-B)>4.7$ and $I=19.67$, $(B-I)=2.06$, $(U-B)>3.3$. Their colours indicate that they are most likely to be $z\gtrsim3$ QSOs, in which case we would estimate a surface density of such objects of ~8 deg^{-2}. The two objects lie in A1758 [α(J2000) = 13 32 23.2, δ(J2000) = +50 34 32] and A2261 [α(J2000) = 17 22 37.4, δ(J2000) = +32 11 19], at radii of 330 and 240 arcsec from the central galaxies. The object in A1758 is also detected as an X-ray source in the PSPC/HRI images of this cluster.

night of 1997 January 31 (Table 1). These frames were reduced in the same manner as the cluster observations. Calibration of these data was provided from observations of Landolt (1992) standard stars, observed before and after the science exposures, giving zero-point errors of $\Delta B = 0.04$ and $\Delta I = 0.05$. We confirm the accuracy of the colours determined from these fields using the locus of stars on the colour–colour plane, as was done for the cluster observations.

The objects in this field were catalogued in a manner similar to that used for the cluster observations, starting with an I-selected sample and measuring colours in seeing-matched apertures. The precision of these colours is similar to that achieved in our cluster observations as a result of equivalent exposure times for the B and I observations. The final catalogue contains 377 galaxies brighter than $I = 22.0$, or a surface density of 4.7 ± 0.5 galaxies arcmin^{-2}, where the variation is estimated from independent sub-regions within the field. As we will show, the clusters studied here are sufficiently rich, given their redshifts, that field contamination only becomes an important correction at the faintest magnitudes discussed. To $I = 20$, the typical cluster frame contains 315 galaxies, of which 90 (28 per cent) are expected to be field contamination, predominantly blue galaxies; this fraction increases to 40 per cent at $I = 22$, the faintest limit used in this work. In our analysis we will ignore the effects on the estimated field correction of gravitational amplification of the background field population. The majority of our analysis focuses on galaxies with red optical colours, and for these we expect the effects of lensing to actually lower the background field density (cf. Broadhurst et al. 1997), leading to a slight over-correction for field contamination.

3 ANALYSIS AND RESULTS

We start by describing the general colour distribution of galaxies within our clusters, before identifying particular groups of objects and discussing their properties in more detail in the following sections.

We show in Fig. 2 the distribution of galaxies on the $(U-B)$–$(B-I)$ colour–colour (c–c) plane in each of the 10 clusters, after correcting for field contamination. We also

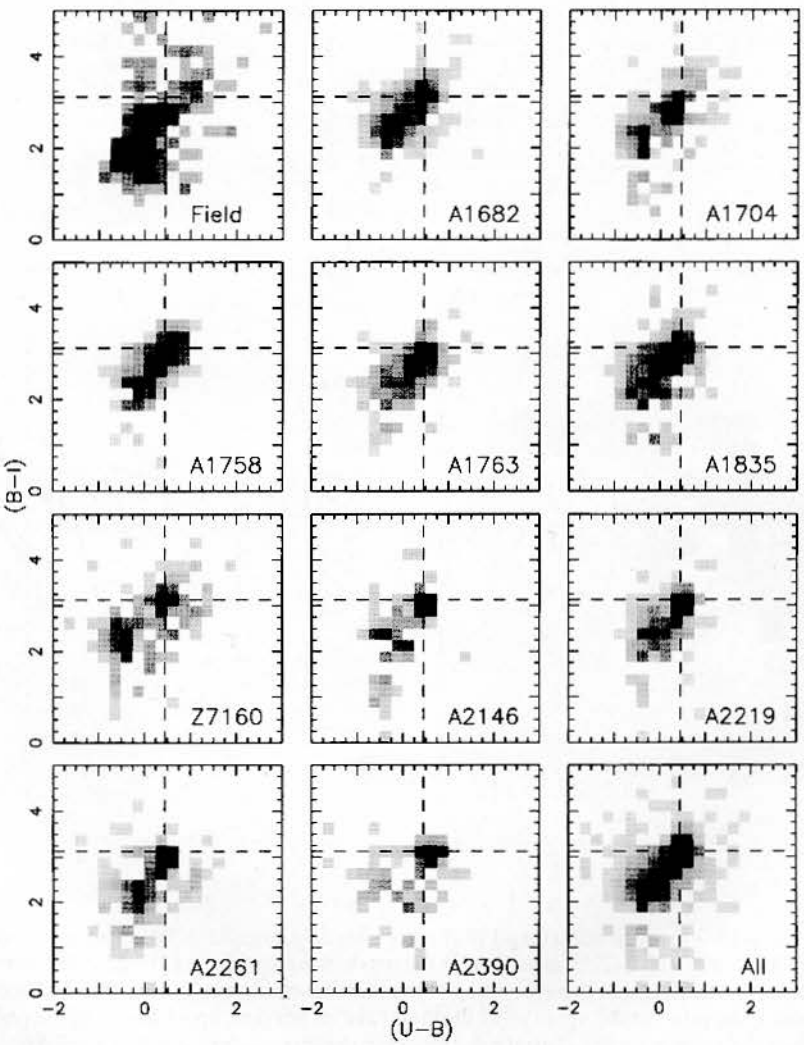

Figure 2. The $(U-B)$–$(B-I)$ colour–colour plane for each cluster showing the distribution of colours for galaxies brighter than $I = 22.0$, after correction for field contamination. We also show the equivalent distribution for the field population, as well as the combined distribution for all the clusters. The dashed lines are to facilitate the comparison of the various distributions.

show the composite colour distribution for all the clusters combined. All of these plots use only those objects classified as galaxies and with magnitudes brighter than $I \leq 22.0$. No differential K-corrections, to compensate for the different cluster redshifts, have been applied to any of these plots. In Fig. 3 we present the combined cluster sample as three independent magnitude slices, along with the whole sample. On these plots we have marked the locus of colours expected for the spectral energy distributions (SED) representative of the spectral types of galaxies with E, Sab, Sbc, Scd and Sdm morphologies in the local Universe (effectively a series of increasing ratios of current to average star formation rate), as they would be observed at $z = 0.24$. It can be seen that the clusters contain galaxies spanning the

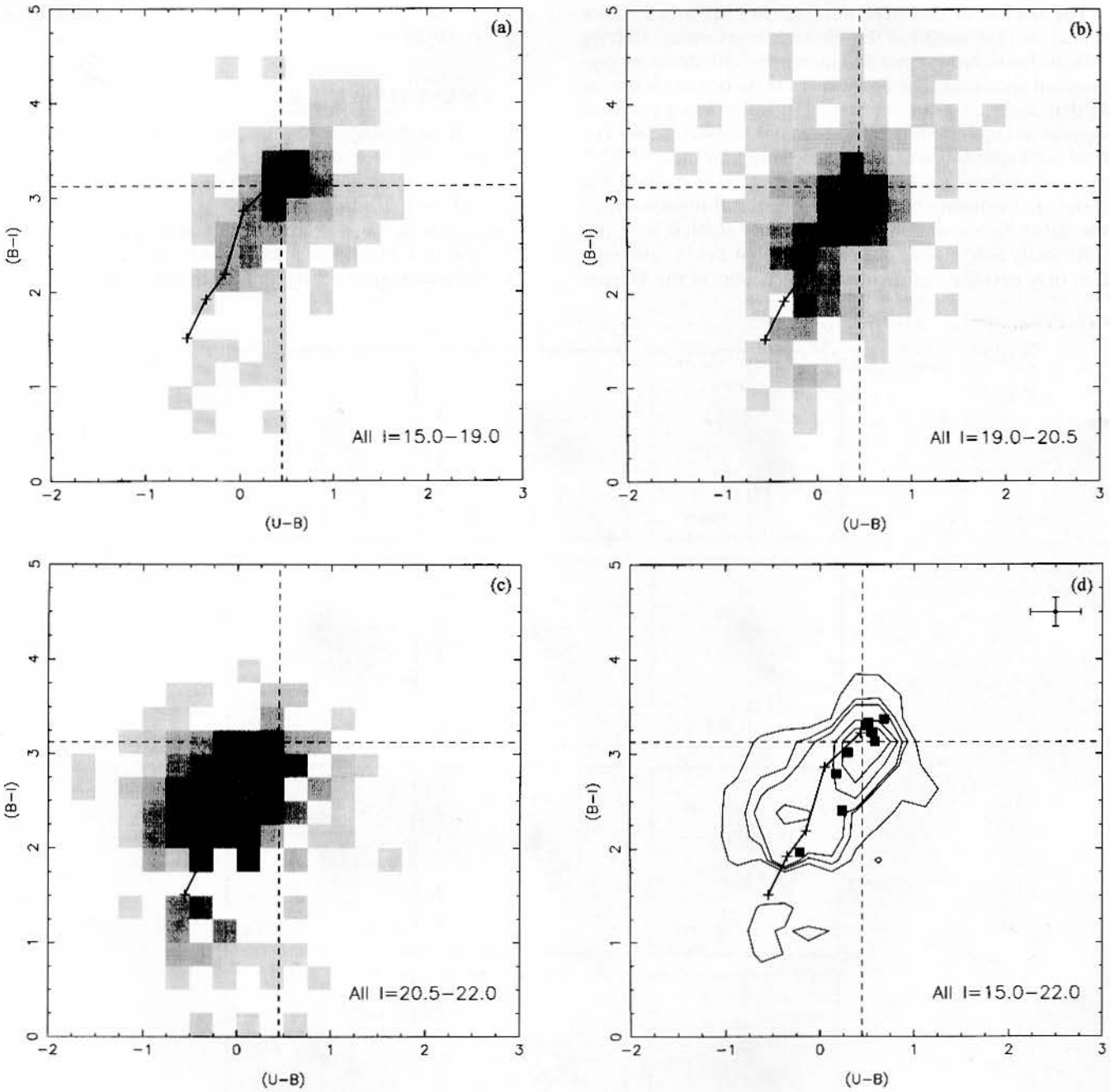

Figure 3. The combined $(U-B)$–$(B-I)$ distribution for all 10 clusters after field correction. We show this for three independent magnitude slices, $I = 15.0$–19.0, $I = 19.0$–20.5 and $I = 20.5$–22.0, as well as for the whole sample with $I = 15.0$–22.0. We also over-lot the locus of colours for the non-evolved spectral energy distributions corresponding to the local spectral types E, Sab, Sbc, Scd and Sdm (upper-right to lower-left). On the $I = 15.0$–22.0 panel, the point at the upper right illustrates the 80 per cent upper limits on the photometric errors at $I \leq 22$. In addition, on this panel we show the colours for the central galaxies of the clusters, measured within a $\sim 7.5\,h^{-1}$ kpc diameter aperture. The three central galaxies with anomalously blue colours are [from the bluest in $(B-I)$] in A1835, A2390 and Zw7160. All these central galaxies also show line emission indicating some level of on-going star formation (Allen 1995). The contours in the final plot are $[0.1,0.5,0.8,2,4,8,12] \times 10^3$ galaxy mag^{-2}.

whole range of star formation rates observed in the local field. At bright magnitudes, however, the distribution is dominated by a population of galaxies with $(U-B)$ and $(B-I)$ colours similar to unevolved elliptical galaxies at these redshifts. As we look at fainter luminosities within the clusters we find a gradual increase in the number of blue galaxies, with colours ranging across those expected from galaxies with star formation rates similar to local Sbc to Sdm galaxies. A similarly wide range in galaxy colours is also seen for the brightest cluster galaxies (Fig. 3); these are typically D or cD galaxies, and although a number of them show the red colours expected for such massive spheroidal systems, three show substantially bluer colours, indicating significant on-going star formation (Allen 1995).

We now identify three groups of cluster galaxies on the $(U-B)$–$(B-I)$ colour–colour plane to $I=22$ and use these to highlight the various components of the cluster populations. At this depth the median photometric errors are $\delta(U-B)=0.11$ and $\delta(B-I)=0.06$, with 80 per cent of the objects having errors less than $\delta(U-B)=0.27$ and $\delta(B-I)=0.15$, adequate to define independent regions of the colour–colour plane. In particular the accuracy of our $(B-I)$ photometry allows us to robustly separate samples of galaxies using this colour, which measures the strength of their 4000-Å breaks. The three groups we identify are: (1) a large population of galaxies with colours similar to passive elliptical galaxies at the cluster redshift; (2) the cluster population with colours typical of star-forming galaxies at $z\sim0.24$; and (3) a number of galaxies whose $(B-I)$ colours indicate a strong 4000-Å break, representative of an evolved stellar population, but which have bluer $(U-B)$ colours than group (1), showing that they are, or recently have been, forming stars. For ease of use we have called these three groups 'Red', 'Blue' and 'UV+'. To estimate the relative proportions of these groups within the clusters we define rough limits of their boundaries on the $(U-B)$,$(B-I)$ colour–colour plane as: [0.1:0.9,2.9:3.6] for Red, [−1.1:0.9,1.9:2.9] for Blue and [−1.1:0.1,2.9:3.6] for UV+. Note that the exact definitions of the samples used in our analysis below vary according to what questions we are attempting to answer; we have used the regions above simply to illustrate the distribution of objects in the various groups. The typical proportions of the three cluster populations are then: [0.95,0.05,0.00] to $M_V=-18.5+5\log h$ and [0.66,0.29,0.05] to $M_V=-17.0+5\log h$. We give the proportions in the individual clusters in Table 2. The average radial distributions of the three galaxy populations in the clusters within $500\,h^{-1}$ kpc of the cluster centres are shown in Fig. 4. Outside of $\sim100\,h^{-1}$ kpc the profile of the Red galaxies drops as $\alpha=-0.96\pm0.08$, close to the value expected for an isothermal distribution. The UV+ population follows a radial distribution close to that of the red galaxies, although with a large scatter, $\alpha=-0.87\pm0.46$, while the Blue galaxy distribution is considerably flatter with $\alpha=-0.46\pm0.20$.

Finally, we can identify one further sample of galaxies on the c–c plane: those galaxies with colours substantially redder than the cluster elliptical sequence in $(B-I)$ (which provides a good measure of the strength of the 4000-Å break at the cluster redshifts). This last group consists of galaxies which are probably background to the cluster, as the elliptical sequence represents galaxies with the strongest 4000-Å breaks at the cluster redshift, and as such we do not discuss them further here. The number of objects lying substantially redward of the cluster sequence in $(B-I)$ is consistent with the number expected from our field distribution.

Table 2. The relative proportions of the various cluster populations we identify, for two absolute magnitude limits. 'Red' galaxies have $(U-B)$,$(B-I)$ colours of [0.1:0.9,2.9:3.6], 'Blue' have [−1.1:0.9,1.9:2.9] and 'UV+' have [−1.1:0.1,2.9:3.6]. These values are for a fiducial cluster at $z=0.24$ and refer to the whole area imaged in each cluster. The relative proportions have been corrected for field contamination.

$M_V \leq -18.5+5\log h$

Cluster	N_{red}	N_{blue}	N_{UV+}	f_{blue}	f_{UV+}
A1682	133.0	2.0	1.7	0.01	0.01
A1704	69.6	−4.4	1.8	−0.07	0.03
A1758	160.1	20.1	1.9	0.11	0.01
A1763	143.3	−3.7	−1.2	−0.03	−0.01
A1835	148.7	11.7	5.0	0.07	0.03
Zw7160	69.3	12.3	0.9	0.15	0.01
A2146	66.0	0.0	−1.3	0.00	−0.02
A2219	180.0	8.0	−0.3	0.04	−0.00
A2261	131.9	12.9	−1.3	0.09	−0.01
A2390	105.0	−5.0	−1.3	−0.05	−0.01
All	1206.9	53.9	5.9	0.04	0.01

$M_V \leq -17.0+5\log h$

A1682	258.9	135.7	47.3	0.31	0.11
A1704	131.0	45.6	7.8	0.25	0.04
A1758	225.0	127.1	8.2	0.35	0.02
A1763	247.4	59.1	14.5	0.18	0.05
A1835	224.4	128.5	45.7	0.32	0.11
Zw7160	108.6	104.6	5.4	0.48	0.02
A2146	94.9	35.7	1.3	0.27	0.01
A2219	307.8	83.7	13.3	0.21	0.03
A2261	184.7	79.3	0.2	0.30	0.00
A2390	118.8	27.6	0.3	0.19	0.00
All	1901.5	826.9	144.0	0.29	0.05

3.1 Red cluster galaxies

The most obvious feature of the $(U-B)$–$(B-I)$ plots in Figs 2 and 3 is the strong clump of red galaxies in all the clusters. The clump is populated with the luminous elliptical galaxies which dominate the bright end of the cluster population. Replotting the catalogues as colour–magnitude (c–m) diagrams illustrates another property of this population – a very narrow colour–luminosity relation in both $(U-B)$–I and $(B-I)$–I (Fig. 5). In both panels the ellipti-

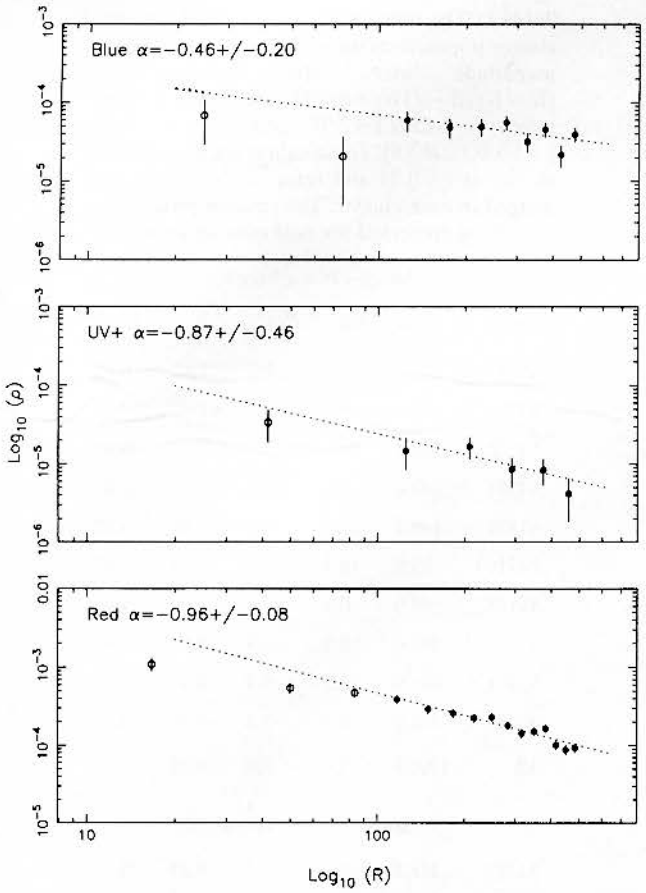

Figure 4. The radial density distributions (in numbers of galaxies per square h^{-1} kpc) of the three galaxy populations ('Red', 'Blue' and 'UV+') identified from the colour–colour planes in Fig. 3. These are shown for a magnitude limit of $M_V = -17.0 + 5\log h$ and have been corrected for field contamination. The bimodal cluster, A1758, is not used in this plot. We fit power laws to the radial distributions outside of $100\,h^{-1}$ kpc; to reduce the effects of crowding on the fits, the points used are marked as filled symbols. The best-fitting power laws are ploted on the figures.

cal sequence slants down, indicating that the spheroidal galaxies have bluer colours at fainter luminosities, a result of lower mean metallicities in the low luminosity galaxies (Kodama & Arimoto 1997). In the fainter samples in Fig. 3, however, this population appears to disperse, a feature which may be associated with the apparent 'break' at $I \sim 20.5$ in the red elliptical sequence on the $(U-B)$–I plane. We return to a discussion of this feature later.

The first question we wish to investigate is the variation in the typical colours of the brighter spheroidal galaxies across the clusters. As we discussed in the introduction, the dispersion in the rest frame UV–optical colours of galaxies is a sensitive test of the recent level of star formation, and the variation of the mean colours for the spheroidal population can give powerful constraints on their formation epoch (BLE; Ellis et al. 1997; Stanford et al. 1998) as well as on the formation of the larger structures inhabited by these galaxies. To study this scatter, we fitted to the colour–luminosity relation in our clusters and then correct these fits to a fiducial cluster at $z = 0.24$ (the mean of our sample) to compare the various values.

We fitted a linear relation $[(U-B) = A(U-B) + B(U-B)I$ or the equivalent for $(B-I)]$ to the c–m relation using the same technique applied by BLE and Ellis et al. (1997): Huber's robust estimator, after removal of probable field contamination. Galaxies are rejected from the fit interactively until the fit is stable to the inclusion of remaining points; the expected number of field galaxies is used as a guide to indicate the numbers of galaxies to be removed (typically 25 ± 5 galaxies, or ~ 10 per cent of the sample). We have confirmed that these fits are not sensitive to modest changes in the definition of the red subsample region on the c–c plane. We then fit the resulting sample across a fixed range in absolute luminosity corresponding to $M_V - 5\log h = [-23.5, -18.5]\,(I \lesssim 20)$. For simplicity we parametrize the variation in apparent magnitude across the redshift range of our sample, for an $M_V = -18.5 + 5\log h$ galaxy with a non-evolved elliptical SED the apparent magnitude is: $I = 17.30 + 10.1z$. The fits are evaluated at an absolute magnitude corresponding to $I = 18$ at $z = 0.24$, roughly M^*. We than apply differential K-corrections to the intercept values to convert them to a cluster observed in $(U-B)$ or $(B-I)$ at $z = 0.24$. The corrections assume a non-evolved elliptical SED and are parametrized as: $K(U-B) = -1.11\Delta z$ and $K(B-I) = -3.14\Delta z$ to 2 per cent accuracy. These corrections amount to $\lesssim 0.05$ in $(U-B)$ and $\lesssim 0.13$ in $(B-I)$, with uncertainties of $\lesssim 0.003$ at a fixed luminosity. The different K-corrections associated with the variation in galaxy colour along the elliptical sequence will introduce a scatter into the corrected colours. From the slope of the c–m relations we expect this to be at the level of $\delta B(U-B) \sim 0.008$ and $\delta B(B-I) \sim 0.006$, where the slope is steeper in both colours at higher redshifts. This is substantially larger than the colour variations introduced between clusters due to our adoption of a fixed aperture size for our photometry, $\delta \lesssim 0.001$, and so we ignore the effects of the variation in metric aperture size across the different clusters. We obtain the fits listed in Table 3(a) and (b) [for $(U-B)$ and $(B-I)$ respectively]. From these we determine average slopes for the c–m sequence of $B(U-B) = -0.041 \pm 0.020$ and $B(B-I) = -0.067 \pm 0.019$, where the scatter within the sample is comparable to the typical errors on the fit. We have therefore simply adopted these average slopes for all the clusters.

Next, to simplify the comparison of the clusters, we fix the relevant slopes at these average values and refit to our data, across two absolute magnitude ranges: $M_V - 5\log h = [-23.5, -18.5]\,(I \lesssim 20)$ and a more restrictive range $M_V - 5\log h = [-23.5, -20.0]\,(I \lesssim 18.5)$. The results of these fits (evaluated at $I = 18$) are listed in Table 4 and we illustrate the values for the complete sample in Fig. 6. These values show a remarkably small dispersion, $A(U-B) = 0.481 \pm 0.068$ and $A(B-I) = 3.129 \pm 0.041$, while for the smaller, bright subsamples we obtain $A(U-B) = 0.487 \pm 0.087$ and $A(B-I) = 3.130 \pm 0.046$. We find no statistically significant correlation between the mean colours in the two passbands.

The typical colours of the bright elliptical cluster population derived above are similar to those expected from a local L* elliptical galaxy placed at $z = 0.24$: $(B-I) = 3.17$ and $(U-B) = 0.42$. The observed colours are offset by $\Delta(U-B) = 0.05 \pm 0.07$ and $\Delta(B-I) = -0.05 \pm 0.04$ compared to these. These offsets are similar to the limits we

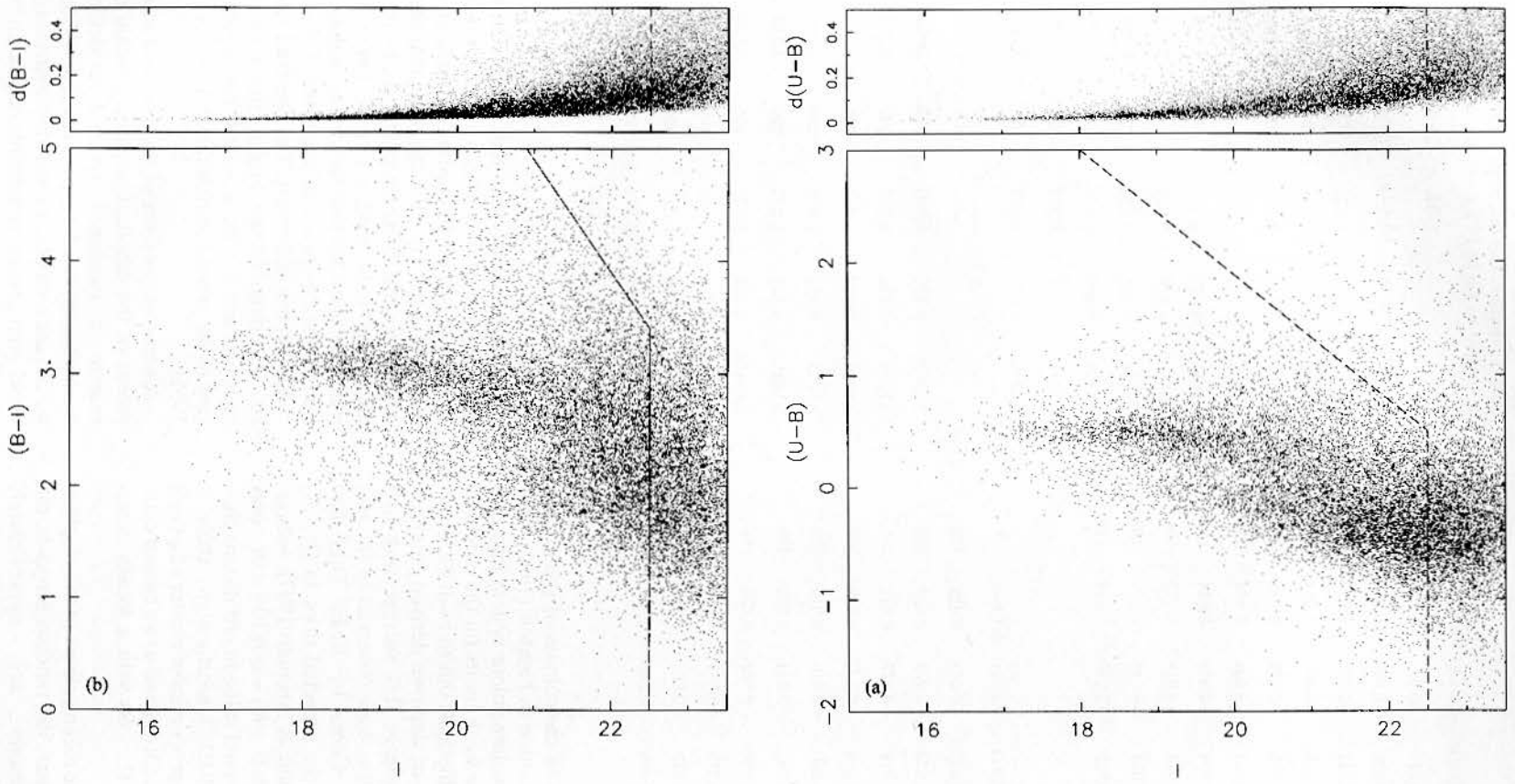

Figure 5. The colour–magnitude distributions for the combined sample of galaxies from the 10 clusters. We have made no attempt to correct the colour–magnitude distributions from the various clusters for their different redshifts and so some blurring of features is expected in this plot. The strong linear feature visible at bright magnitudes in both plots is a result of the red elliptical cluster members. Note the apparent decline in the number of galaxies lying on this sequence in the $(U-B)$–I plot at $I \gtrsim 20.5$. The dashed lines show the 80 per cent completeness limits for the various catalogues, these roughly correspond to a typical photometric accuracy of ~ 0.2 mag in each band. No correction has been made for field contamination in this figure.

Table 3. The coefficients of linear fits to the $(U-B)$–I and $(B-I)$–I c–m for red cluster galaxies. The intercept values are evaluated at a magnitude equivalent to $I=18$ in a $z=0.24$ cluster.

Cluster	z	$A_{(U-B)}$	$\delta A_{(U-B)}$	$B_{(U-B)}$	$\delta B_{(U-B)}$	N
A1682	0.226	0.473	0.017	−0.021	0.016	177
A1704	0.220	0.399	0.020	−0.026	0.018	107
A1758	0.280	0.588	0.017	−0.070	0.017	206
A1763	0.228	0.500	0.015	−0.055	0.014	209
A1835	0.253	0.444	0.018	−0.032	0.018	200
Zw7160	0.256	0.370	0.024	−0.031	0.026	126
A2146	0.234	0.493	0.024	−0.044	0.025	100
A2219	0.228	0.501	0.013	−0.018	0.012	230
A2261	0.225	0.456	0.016	−0.044	0.015	197
A2390	0.233	0.638	0.019	−0.075	0.018	198

Cluster	z	$A_{(B-I)}$	$\delta A_{(B-I)}$	$B_{(B-I)}$	$\delta B_{(B-I)}$	N
A1682	0.226	3.225	0.021	−0.062	0.019	173
A1704	0.220	3.048	0.020	−0.073	0.018	100
A1758	0.280	3.088	0.019	−0.077	0.021	216
A1763	0.228	3.085	0.018	−0.100	0.018	202
A1835	0.253	3.098	0.016	−0.046	0.016	195
Zw7160	0.256	3.073	0.031	−0.044	0.031	109
A2146	0.234	3.105	0.020	−0.092	0.020	89
A2219	0.228	3.138	0.015	−0.049	0.014	221
A2261	0.225	3.034	0.013	−0.067	0.013	163
A2390	0.233	3.121	0.020	−0.066	0.019	194

Table 4. The intercepts of fits to the c–m relations in the clusters adopting a fixed slope in each passband [$B(U-B)=-0.041$ and $B(B-I)=-0.067$]. These are shown for the two magnitude-limited samples. The intercept values are evaluated at a magnitude equivalent to $I=18$ in a $z=0.24$ cluster.

$M_V \leq -20.0+5\log h$

Cluster	$A_{(U-B)}$	$\delta A_{(U-B)}$	$N_{(U-B)}$	$A_{(B-I)}$	$\delta A_{(B-I)}$	$N_{(B-I)}$
A1682	0.472	0.022	37	3.219	0.019	31
A1704	0.389	0.028	27	3.085	0.022	21
A1758	0.606	0.016	50	3.133	0.014	43
A1763	0.490	0.022	42	3.135	0.019	36
A1835	0.440	0.018	44	3.114	0.014	36
Zw7160	0.379	0.032	34	3.140	0.032	17
A2146	0.485	0.023	27	3.098	0.017	26
A2219	0.486	0.015	51	3.170	0.017	42
A2261	0.458	0.017	52	3.057	0.014	45
A2390	0.660	0.021	47	3.150	0.017	38

$M_V \leq -18.5+5\log h$

A1682	0.487	0.013	177	3.210	0.009	173
A1704	0.423	0.016	107	3.086	0.009	100
A1758	0.557	0.013	206	3.125	0.009	216
A1763	0.481	0.010	209	3.115	0.007	202
A1835	0.444	0.013	200	3.133	0.007	195
Zw7160	0.373	0.016	126	3.125	0.012	109
A2146	0.475	0.016	100	3.112	0.012	89
A2219	0.506	0.011	230	3.171	0.006	221
A2261	0.446	0.014	197	3.068	0.008	163
A2390	0.614	0.013	198	3.149	0.010	194

placed on the relative offset of the colours of stars in our fields compared to the distribution in Landolt (1992). Taking the uncertainty in our absolute colour system into consideration, we can only place weak limits on the extent of colour evolution of cluster ellipticals out to $z=0.24$. Looking at the average $(B-I)$ c–m slope we derived from our clusters, we can crudely compare this average with that measured in $(U-R)$ using the slope observed in $(U-V)$ for spheroidal galaxies in Coma by BLE. They find $B(U-V)=-0.082\pm0.008$, the expected slope in $(V-R)$ is $B(V-R)\sim-0.020$ (Kodama & Arimoto 1997), indicating a predicted slope of $B(U-R)=-0.10\pm0.01$, only slightly steeper than the observed value in our distant clusters of $B(B-I)=-0.07\pm0.02$. Unfortunately, there is little information on the UV properties of cluster ellipticals shortward of the atmospheric cut-off and so we cannot compare the observed slope in $(U-B)$ with a locally determined value.

Turning to the scatter in the mean colours of the elliptical sequences between the clusters, the random errors in the calibration of the clusters are approximately $\delta(U-B)=0.053$ and $\delta(B-I)=0.034$; removing these contributions from the observed scatter would indicate intrinsic 1σ dispersions of $\delta(U-B)\lesssim0.04$ and $\delta(B-I)\lesssim0.02$. We therefore conclude that the red, spheroidal populations brighter than $M_V=-18.5+5\log h$ are remarkably homogeneous across all 10 clusters in our sample at a lookback time of $\sim2\,h^{-1}$ Gyr. We also note that the small spread in colours for the brighter ellipticals in the clusters would allow them to be used as a crude, but economical, redshift indicator, provided that the colour evolution of the population can be calibrated for a number of clusters spanning the redshift range of interest. The observed scatter in the mean $(B-I)$ colour of the bright cluster ellipticals, including measurement errors, is ~0.04, corresponding to an accuracy in the estimated redshift of $\Delta z\sim0.01$ (cf. Belloni et al. 1995).

A complete analysis of the expected scatter in the mean colour of the elliptical sequences within rich clusters will require a combined spectral modelling and Press–Schechter approach (e.g. Baugh et al. 1996b). Nevertheless, we can use a simple, if somewhat contrived, model to understand what general constraints our observations provide on the discreteness of the structures which coalesce to form rich clusters. In the model, clusters from subunits (groups) of galaxies each containing a fixed number of elliptical

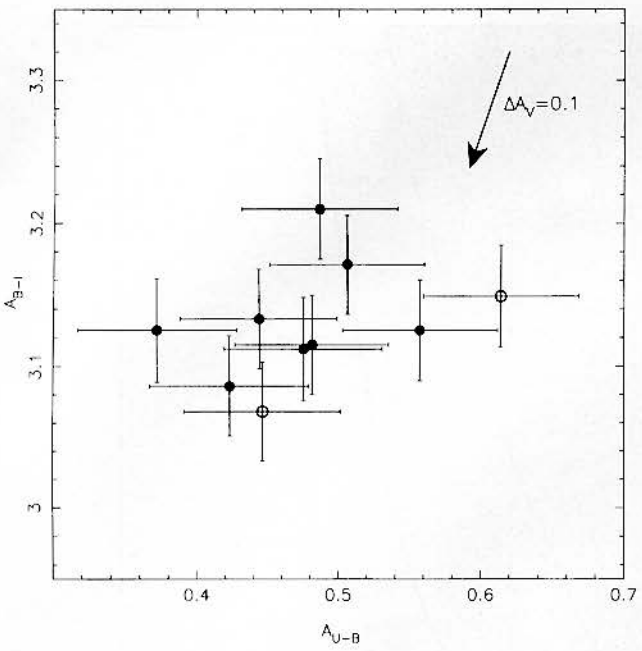

Figure 6. The intercepts for the c–m relations in the different clusters (Table 4), evaluated at a fiducial magnitude equivalent to $I=18$ at $z=0.24$ and corrected for differential K-corrections assuming a non-evolved elliptical SED. The two open symbols mark A2390 and A2261, where the photometry was corrected using the stellar sequences in the CCD frames. The vector indicates the effect of changing the adopted reddening and we have included the expected random calibration errors for the clusters in their error bars.

galaxies, N_E. The elliptical galaxies within a given group have synchronized formation at some epoch (this could be thought of as relating to the collapse redshift of the group) which we distribute uniformly in time between the Big Bang and a cut-off time, t_{End}, when elliptical formation ceases in all structures. We define t_{End} relative to $z=0.24$ and hence $t_{End}=0$ means that elliptical formation continues right up to $z=0.24$, while $t_{End}=5$ Gyr ($h=0.5$) corresponds to a time 5 Gyr prior to $z=0.24$, or roughly $z_F\sim 1$. In the Press–Schechter models, the redshift cut-off and the distributions in relative formation times for ellipticals within the groups would probably both be functions of group mass, as well as cosmology, but the current model is sufficient to illustrate the technique. We now determine what joint constraints our observed cluster-to-cluster scatter in $(B-I)$, rest frame $(U-R)$, provides on the numbers of structures from which the clusters, were built, and the most recent epoch of elliptical formation in these structures. We use the spectral evolution model of Fioc & Rocca-Volmerange (1998) for elliptical galaxies to determine the evolution in the rest frame $(U-R)$ colours of the galaxies. Starting from the observed number of ellipticals in the cluster, we randomly select groups of N_E galaxies and assign them a formation epoch uniformly in the available time interval – from this we determine their $(U-R)$ colour at $z=0.24$. We repeat this until we have fully populated the cluster and then calculate the mean colour of the elliptical population in the cluster before moving on to the next cluster, until all have their full complements of elliptical galaxies. With values for the mean colours of the elliptical population in each of the 10 model clusters, we next estimate the scatter in the colours *between* the clusters. This procedure is repeated 10000 times for each combination of N_E and t_{End} to estimate the likelihood that the scatter amongst the 10 model clusters would be less than or equal to that observed for those parameters.

Looking at Fig. 7 it is apparent that as we form the cluster from larger and larger subunits (higher N_E) then the scatter between the clusters should increase. Remembering that all the galaxies within a given subunit form together, but that the subunits themselves can form at any point within the available time period, we can see that this constraint arises from the increasing shot noise in the average colour of the cluster population when it is formed from a smaller and smaller number of independent subunits. At one extreme, where each cluster forms as a single group of ellipticals ($N_E \gg 1$) which all formed together at a given time, then the scatter between the clusters simply reflects the scatter between the formation times of the original groups and these are therefore constrained to all have formed in a relatively short period of time (to minimize the scatter between their present-day colours). Such a model might represent the result of a top-down formation of clusters from large Zel'dovich pancakes, with the bright ellipticals being formed in the first collapse. Looking at Fig. 7 we could constrain the elliptical formation to occur at least $t_{End}\sim 6$–7 Gyr ($h=0.5$) before $z=0.24$ or $z_F \gtrsim 2$. At the other extreme, where the clusters form from accreting individual elliptical galaxies ($N_E\sim 1$) the formation epochs of which are uncorrelated, we see that given the large number of ellipticals within each cluster the mean colours of the clusters have a very small scatter and hence the constraint on the last period of star formation in the elliptical population is much weaker (equivalent to $z_F \gtrsim 0.5$). Taking an intermediate case, if the clusters typically form from sub-clumps and groups containing ~ 10 ellipticals, and the formation of the galaxies within each group is synchronized, then these structures must have formed their galaxies at least 5 Gyr ($h=0.5$) before $z=0.24$ [95 per cent confidence limits (c.l.)], equivalent to $z_F \gtrsim 1$. Requiring that the bulk of the ellipticals form much earlier than this (e.g. $z\gtrsim 3$, Ellis et al. 1997) would mean that we could only rule out their coherent, stochastic formation in large structures ($N_F\sim 20$).

The colours of the bright cluster ellipticals indicate that this population is remarkably homogeneous between clusters. We can further test this homogeneity by investigating the scatter in the amount of baryonic material locked up as stars in the cluster ellipticals, as compared to the total mass of the cluster. The simplest method by which to achieve this is to compare the luminosity in the elliptical sequence to the cluster X-ray temperatures for the seven clusters with published temperatures (Mushotzky & Scharf 1997). We determine the total spheroidal luminosity in our cluster by simply integrating the light in the cluster sequences defined above down to $M_V=-18.5+5\log h$ across the whole field (an effective radius of 0.75 h^{-1} Mpc in a typical cluster). The values obtained, along with a bootstrap estimate of their uncertainties, are given in Table 5. We find a reasonable linear correlation (Fig. 8) between the integrated red galaxy luminosities and the X-ray temperatures: $L_E=(0.47\pm 0.08)\times 10^{12}\ T_X$, where the fit has been constrained to pass through [0,0]. The dispersion around this

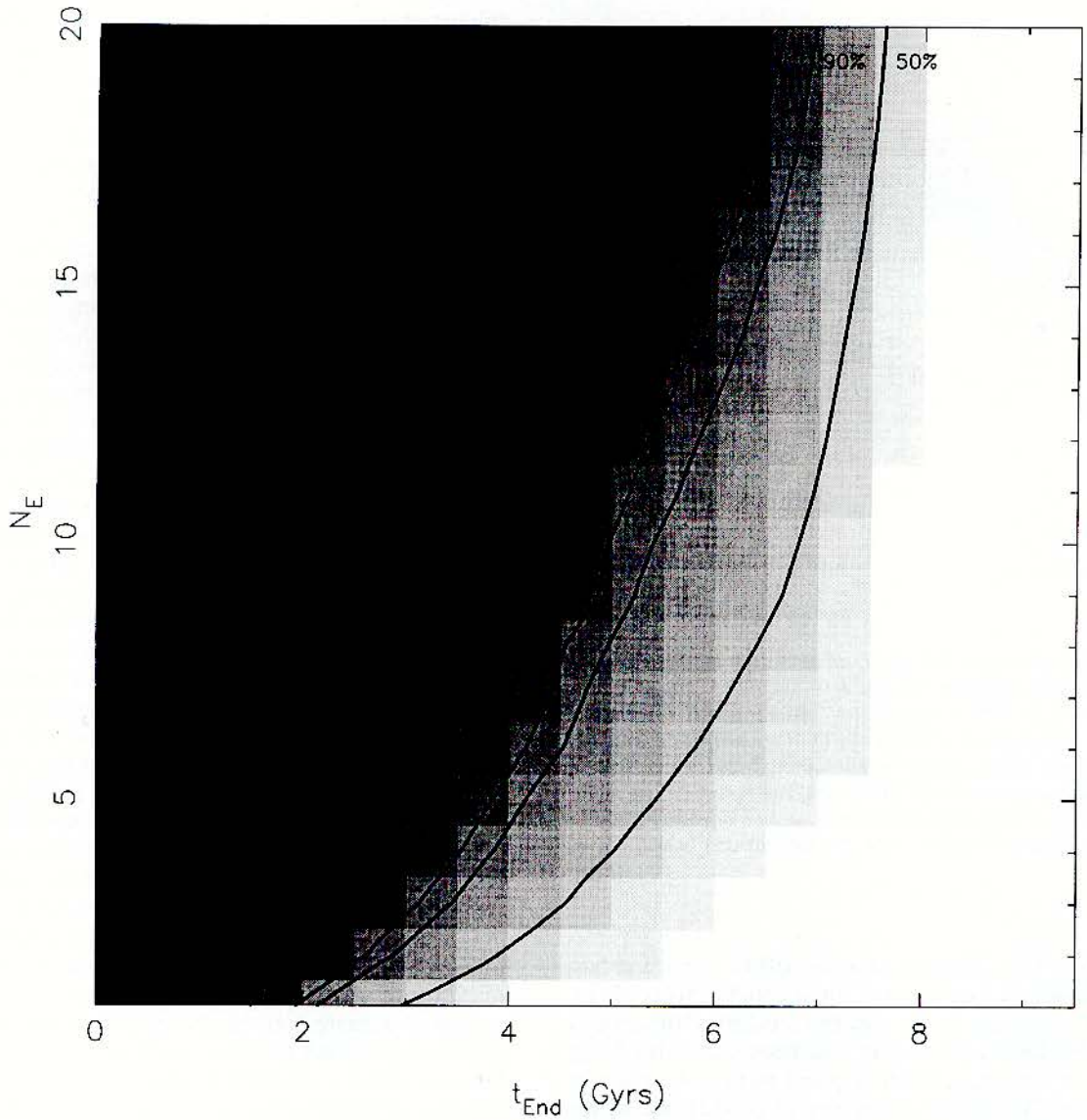

Figure 7. The logarithmic likelihood distribution for the two free parameters of our simple model of cluster formation: N_E, the number of ellipticals in a typical group accreted by the cluster; and t_{End}, the time before $z=0.24$ when elliptical formation stops in all structures. The contours show the probabilities that the scatter between the clusters would be less than the observed value, and mark the 50, 90, 95 and 99 per cent confidence limits. Thus the lighter area to the right of the figure indicates the allowed region of the parameter space. For example, if the clusters form from groups containing ~ 10 coeval ellipticals, $N_E=10$, then these structures must have formed their galaxies earlier than $t_{End} \gtrsim 4$–5 Gyr before $z=0.24$ (95 per cent c.l.), equivalent to $z_F \gtrsim 1$. Here we have used the brighter sample of cluster ellipticals (Table 4) to constrain the model and assumed a $h=0.5$ and $\Omega_0=1$ cosmology which gives an age of the Universe of 9.5 Gyr at $z=0.24$.

line is small, only 17 per cent (compared to ~ 30 per cent when L_X is used in place of T_X), indicating that the integrated luminosity of the red galaxy population is a good tracer of the total mass of the cluster. In fact the 'true' scatter may be less when proper account is taken of the roles of mergers and cooling flows in changing the observed X-ray temperatures. Parametrizing the ratio of the cluster mass to the luminosity of the elliptical population as: $M/L_E=\gamma h(M/L_V)_\odot$, and assuming an isothermal gas distribution with $\beta_{fit}=1$, we find $L_E=(81\times 10^{12}\,T_X)\gamma$ for L_E in solar units and T_X in keV. Thus the observed best-fitting slope corresponds to $M/L_E=(170\pm 30)h$ in the rest frame V-band. Including the observed passive evolution of the stellar populations (see Section 3.2), this corresponds to an equivalent $z=0$ value of $M/L_E=(220\pm 40)h(M/L_V)_\odot$. This compares well to the value for the Coma cluster of $M/L_V=240h(M/L_V)_\odot$ within $0.5\,h^{-1}$ Mpc (transformed from the B-band value of Fusco-Femiano & Hughes 1994).

3.2 The 'UV + ' cluster population

While the proportion of galaxies falling in the UV + region of Fig. 3 is small at bright magnitudes, constituting only ~ 0.5 per cent of the cluster population brighter than $M_V \sim -18.5+5\log h$, it substantially increases as we reach fainter into the cluster population (Table 2). The colour

Table 5. The structural parameters of the clusters determined from our galaxy catalogues.

Cluster	C	R_{30} (arcmin)	N_{30}	L_V ($h^{-2}10^{10}L_\odot$)	f_b
A1682	0.32	1.75	45	368 ± 30	-0.01 ± 0.05
A1704	0.63	1.18	21	243 ± 24	0.10 ± 0.10
A1758[1]	0.45	2.10	65	536 ± 54	0.08 ± 0.06
A1763	0.44	1.75	53	432 ± 32	0.03 ± 0.05
A1835	0.42	1.37	52	487 ± 40	0.00 ± 0.03
Zw7160	0.37	2.22	36	204 ± 15	0.08 ± 0.10
A2146[2]	0.45	0.80	14	246 ± 21	-0.07 ± 0.02
A2219	0.40	1.56	60	470 ± 23	0.08 ± 0.05
A2261	0.32	2.13	66	424 ± 30	0.20 ± 0.08
A2390	0.38	1.37	49	441 ± 29	0.05 ± 0.05

[1] C, R_{30}, N_{30} and f_b calculated using south-east component as centre.
[2] C, R_{30}, N_{30} and f_b calculated using the mean of the position of the two bright galaxies as centre.

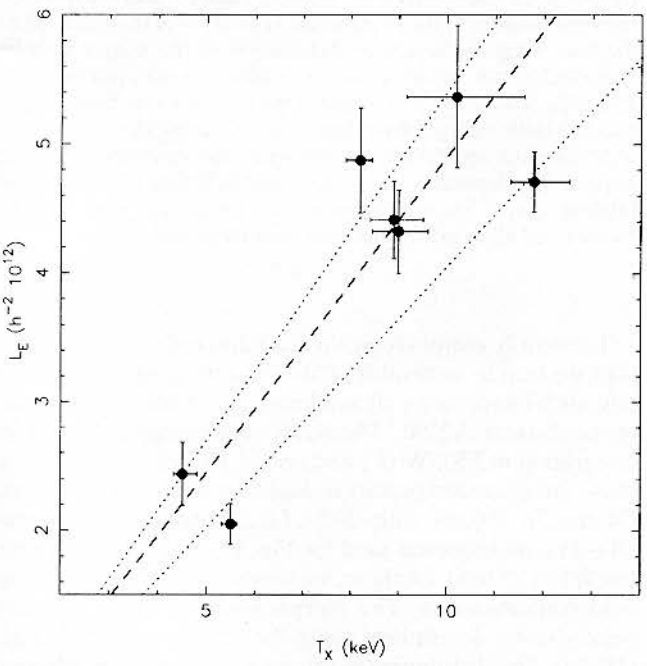

Figure 8. The correlation between the integrated optical luminosities of the elliptical populations in seven of the clusters and their X-ray temperatures. Errors are 1σ for both observables. The dashed line shows the best-fitting linear relationship (constrained to pass through [0,0]). The slope of this line corresponds to a V-band rest frame $M/L_E = (170 \pm 30)h$ in solar units within an effective radius of 0.75 h^{-1} Mpc, the upper and lower dotted lines indicate the relationships for $M/L_E = 150h(M/L_V)_\odot$ and $M/L_E = 200h(M/L_V)_\odot$, respectively.

selection used to define this sample is sufficiently wide that it will include all cluster galaxies with strong 4000-Å breaks (E–S0–Sa), which also show blue $(U-B)$ colours. The accuracy of our $(B-I)$ colours means that we expect little

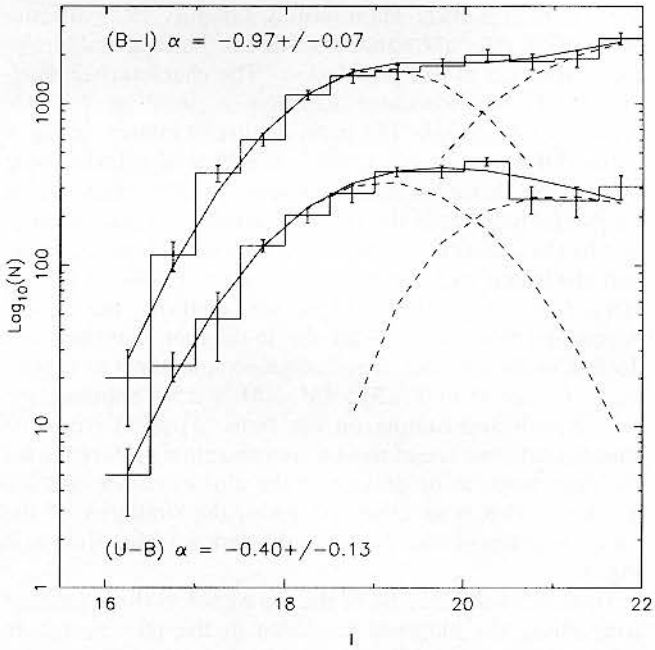

Figure 9. The LF function for galaxies in the red elliptical sequence in the c–m, as identified independently from the $(U-B)$ and $(B-I)$ c–m diagrams (Fig. 5). Notice the relatively flat distribution at the faint end in the $(U-B)$ sample, with an apparent dip in the counts fainter than $I \sim 20.5$ ($M_V = M^* + 2.5$). The composite Gaussian + Schechter function fits to the distributions are plotted as solid curves, with the individual components given as dashed lines. The two LFs have been offset vertically for clarity.

contamination of the sample from later spectral types (with bluer 4000-Å colours). We now investigate the relation between this population and the apparent break in the c–m relation for the cluster ellipticals in $(U-B)$–I. To do this we first look at the luminosity distribution of galaxies lying along the elliptical c–m sequences defined above. We select a wedge-shaped region parallel to the c–m sequence with a width varying from $\Delta(B-I) = 0.18$–0.33 [$\Delta(U-B) = 0.28$–0.43] from $I = 16.0$–22.0; the increasing width of the region at fainter limits compensates for the increased photometric errors. These regions contain 90 per cent of the morphologically classified E and S0 galaxies brighter than $I = 20.5$ in the *HST*/WFPC-2 image of A2390 (see Section 4). Using these areas we determine counts from the combined cluster sample and correct these using the same regions of the field galaxy colour–magnitude plane. The magnitudes and colours for the cluster galaxies are corrected to those of a fiducial cluster at $z = 0.24$ using the K-corrections suitable for a non-evolved elliptical SED (consistent with the typical colours observed for this population).

We plot the luminosity distributions determined from both colour–magnitude planes (Fig. 9). To parametrize the differences between these two luminosity functions (LFs) we have fitted composite Gaussian + Schechter functions (e.g. Wilson et al. 1997) to the distribution, and these are over-plotted in Fig. 9. The only free parameter in the fit is the faint-end slope of the Schechter function. The parameters of the Gaussian function ($I_{cent} \sim 19.1$ and $\sigma \sim 1.4$) have been fixed to agree with the luminosity function of elliptical galaxies in local clusters (Binggeli, Sandage & Tammann

1985, hereafter BST; Thompson & Gregory 1993; Biviano et al. 1995), after allowance is made for the expected luminosity evolution of this population.[3] The characteristic magnitude of the Schechter function is fixed at $I=20.5$, $M_V=-17.7+5\log h$. The main feature of interest in Fig. 9 is the difference in the relative numbers of galaxies lying on the red cluster sequence beyond $I\geq 20.5$, there being considerably fewer in the $(U=B)$ sequence. This is quantified by the different values of the faint-end slope, α, determined for the two samples, $\alpha(U-B)=-0.40\pm0.13$ and $\alpha(B-I)=-0.97\pm0.07$. Thus we confirm the visual impression from the $(U-B)$–I c–m diagram that there is a decline in the number of red sequence members at magnitudes fainter than $I\sim 20.5$ ($M_V\sim M^*+2.5$). Splitting the $(U-B)$-selected sample on the basis of radius from the cluster centre we see at most a very marginal preference for the decrement to be greater in the cluster centre ($r\leq 250\ h^{-1}$ kpc). This is as expected, given the similarity of the radial profiles of the UV+ and Red galaxies shown in Fig. 4.

To search for the cause of the dip we select those galaxies lying along the elliptical sequence in the $(B-I)$–I c–m plane and study the distribution of their $(U-B)$ colours. We show in Fig. 10 the distributions for two independent magnitude slices, $I=19.0$–20.5 and $I=20.5$–22.0, which bracket the position of the dip. The median photometric errors for galaxies within these two samples are $\delta(U-B)=0.08$ and $\delta(U-B)=0.19$. We show the observed distributions in $(U-B)$ colours in Fig. 10; the galaxies lying at $(U-B)\leq 0.1$ are those which correspond to the original definition of 'UV+'. The two samples have intrinsic dispersions of $\delta(U-B)=0.23$ and $\delta(U-B)=0.65$ after removing the contributions from the photometric errors on the objects and the cluster-to-cluster variations in mean colours. Restricting the initial $(B-I)$ selection to cover a similar colour range for the samples brighter and fainter than $I=20.5$ does not reduce the $(U-B)$ colour range seen for the $I>20.5$ sample. Further splitting the $I=20.5$–22.0 sample on the basis of $(B-I)$ colours, we confirm that both halves show similar median $(U-B)$ colours as well as dispersions: $<(U-B)>=0.31\pm0.44$ and $<(U-B)>=0.34\pm0.47$ for the redder and bluer halves respectively, indicating that there is no strong colour–colour correlation within this subsample. We therefore conclude that the red galaxies fainter than $M_V\sim -17.7+5\log h$ have a substantially broader range of mid-UV colours than those galaxies brighter than this limit.

[3]To determine the amount of luminosity evolution in the bright galaxies clusters we use a simple Schechter function fit to the luminosity distribution and then compare the value of M^* we derive with that given by Colless (1989) for the distributions in 14 rich clusters, where he estimated $M^*_{b_j}=(-19.84\pm0.06)+5\log h$ for $\alpha=-1.25$, or $M^*_V\sim -20.5+5\log h$ assuming a mean colour of $(b_j-V)\sim 0.7$. We therefore fit a single Schechter function to our distributions having fix $\alpha=-1.25$ and estimate $I^*=17.40\pm0.07$ from our $(U-B)$ distribution and $I^*=17.42\pm0.06$ from $(B-I)$. These correspond to $M_V=(-20.8\pm0.1)+5\log h$, or $\sim 0.3\pm0.1$ mag brighter than the $z=0$ value. This is in good agreement with the expectation from luminosity evolution of a passively evolving stellar population formed at high redshift ($\Delta M_V\sim -0.3$, Section 3.3; Barger et al. 1998).

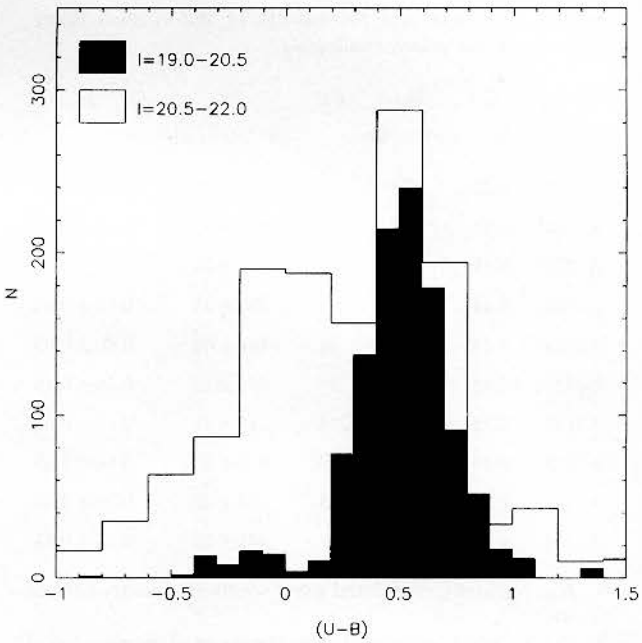

Figure 10. The distribution in $(U-B)$ colour for galaxies lying on the elliptical sequence in the $(B-I)$–I c–m diagram. This is shown for two magnitude ranges, $I=19.0$–20.5 and $I=20.5$–22.0, which span the position of the break in the $(U-B)$ c–m sequence. Note the blue wing to the colour distribution of the fainter sample, compared to the relatively narrow distribution seen just brighter. This wing contains ~ 50 per cent of the population at fainter magnitudes. Both samples have been selected using the same fixed-width envelope around the c–m sequence and are corrected for the slope of the elliptical c–m sequence and field contamination. The brighter sample has been renormalized for the purposes of comparison and all negative bins have been truncated.

To identify morphologically the faint, red cluster population, we turn to archival *HST* WFPC-2 imaging. Unfortunately, such images are only available for a small region in one of our clusters, A2390.[4] The A2390 data comprises an 8.4-ks integration in F555W (V) and one at 10.5 ks in F814W (I): these are discussed further in Kneib et al. (in preparation). Of the 78 objects with $20.5\leq I\leq 22.0$ which fall on the $(B-I)$ c–m sequence used for Fig. 10, only nine lie within the WFPC-2 field. Of these, we would expect 1.6 ± 0.6 to be field contamination. The morphologies of these galaxies were visually determined using the scheme of Smail et al. (1997a). The distribution is three Es, three S0s, an S0/a, an Sc and a gravitationally lensed arc (the giant arc in A2390). The colours of the arc are at the blue end of the distributions, especially in $(U-B)$, while the Sc galaxy is the reddest of the nine galaxies in $(B-I)$, but the second bluest in $(U-B)$ (after the arc), indicating that it is likely to be background. Ignoring these field objects, the remaining seven galaxies split roughly equally into S0 and E. With only three galaxies in each class (we remove the S0/a), our conclusions are limited; however, we note that the S0 galaxies tend to be bluer in both $(U-B)$ [$<(U-B)>_{S0}=0.58\pm0.16$ versus $<(U-B)>_E=0.77\pm$

[4]Very shallow images (~ 0.3 ks) of an area of A1758 have been taken but these are useless for our purposes.

0.06, where the errors on the means are bootstrap estimates] and $(B-I)$ [$<(B-I)>_{S0}=3.01\pm0.08$ versus $<(B-I)>_{E}=3.18\pm0.06$], as well as spanning a wider range in $(U-B)$ colours than the ellipticals, $\sigma_{S0}=0.34$ as opposed to $\sigma_{E}=0.12$. To determine the significance of this difference in the dispersions, we simulate a Gaussian distribution with a dispersion equal to that of the combined E + S0 sample and ask how often we expect the ratio of the relative dispersions of random subsets of three galaxies to exceed that observed ($\sigma_{S0}/\sigma_{E}=2.8$). This occurs in only 2 per cent of cases, which would imply that there may be a real difference between the $(U-B)$ colour ranges of E and S0 galaxies. We conclude that the majority of the cluster galaxies with $I\geq20.5$ and red $(B-I)$ colours are spheroidal systems (E or S0) and that the bluer half of these contains 70 per cent S0 galaxies.

The relatively strong 4000-Å breaks in the UV + galaxies means that in the absence of dynamical effects, we would expect them to undergo only modest fading in their rest frame optical luminosities between $z\sim0.24$ and today, not much above that expected for the elliptical population, $\Delta M_{V}\sim-0.3$. We therefore would predict that this group would contribute $\sim$50 per cent of the population, with strong 4000-Å breaks at typical luminosities of around $M_{V}\sim-17.4+5\log h$ in massive local clusters. We compare the expected characteristics of this population with those observed for different local cluster galaxies in Section 4.

3.3 Blue cluster galaxies

After the red spheroidal sequence, the next most prominent feature in Figs 3 and 5 is the population of faint blue galaxies. While some proportion of these objects in Fig. 5 will be field galaxies, the distributions shown in Fig. 3 have been corrected for this contamination and hence the population of blue galaxies seen there is associated with the cluster, although they do not show the strong central concentration of the red population (Fig. 4).

First we determine the blue fractions (f_{b}) in our clusters, following the prescription of Butcher & Oemler (1984, hereafter BO84). They estimate the radius in the cluster which contains 30 per cent of the population brighter than $M_{V}=-18.5+5\log h$. Using this radius they then calculate the fraction of the $M_{V}\leq-18.5+5\log h$ population within that aperture which have rest frame $(B-V)$ colours bluer than 0.2 mag below the elliptical sequence. Defining the cluster centre from our X-ray images, and correcting for the field counts, we determine the values for R_{30} and N_{30}, the number of cluster galaxies within this radius, given in Table 5. Table 5 also gives the concentration index, $C=\log R_{60}/R_{20}$, as defined by BO84. The only remaining step is to determine the equivalent colour boundary for our passbands. We have the colour of the elliptical sequence in each cluster (Section 3.1), we need to transform an offset of $(B-V)=0.2$ in the rest frame into a difference in the observed $(B-I)$ colour at $z\sim0.24$. For this purpose we simply fit the variation in rest frame $(B-V)$ colour with observed $(B-I)$ colour for the non-evolved SEDs used earlier. From these fits we can derive the $(B-I)$ offset which provides the equivalent colour difference in the rest frame $(B-V)$. A colour of $(B-V)_{E}-0.2$ is between an Sab and Sbc SED (0.67 Sab + 0.33 Sbc) and equivalent to an offset of $\Delta(B-I)=-0.58$ from the observed elliptical c–m sequence. Using this limit and the observed elliptical sequences we determine the blue fractions given in Table 5. We have one cluster in common with the original BO84 study: A1758. For this we derive $C=0.45$, $R_{30}=2.1$ arcmin and $f_{b}=0.08\pm0.06$, in good agreement with the values published by BO84: $C=0.49$, $R_{30}=2.4$ arcmin and $f_{b}=0.09\pm0.04$.

The median f_{b} for the concentrated clusters in our sample, those with $C_{30}\geq0.35$, is $<f_{b}>=0.04\pm0.02$. This is slightly lower than the value of $<f_{b}>=0.09\pm0.04$ for a similar sample of $z=0.2$–0.3 clusters in Butcher & Oemler's original work, perhaps indicating a tendency for these massive clusters to contain a smaller proportion of active galaxies than typically seen in a broad range of collapsed structures at these epochs. It should be a goal of any future studies to investigate such possibilities by contrasting the properties of galaxy populations across a range of environments (cf. Abrahams et al. 1996) in massive and less massive structures at a single epoch. While the individual cluster cores contain so few luminous blue galaxies (typically 2–3 per cluster) that the individual values of f_{b} are not well determined, the presence of such a small number of star-forming galaxies in the core regions of these clusters does mean that they do not show any Butcher–Oemler effect.

The scatter in our $C\geq0.35$ sample is considerable, $\Delta f_{b}=0.06$, and somewhat intriguing given that the clusters are all concentrated and in addition span both a small range in mass and a restricted redshift range. Looking at the concentrated clusters with the two highest f_{b} values (we ignore the two $C\leq0.35$ clusters), we can see no obvious distinction between them and the remainder of the sample. Similarly, focusing on the most bimodal cluster, A1758, we also see no indication of atypical blue fractions in this system. Evidence has been presented for recent mergers in both A2219 (Smail et al. 1995b) and A2390 (Pierre et al. 1996) from detailed lensing analysis, although the blue populations in neither cluster show any strong evidence for a recent influx of star-forming galaxies. We conclude that the wide range in f_{b} seen in our sample probably results from small accretion events which, while adding a few star-forming galaxies to the cluster, do not substantially alter its morphology, mass or X-ray luminosity. This is not to say that the accretion of a more massive structure would not effect the cluster, just that such events appear not to substantially alter the mix of galaxies in the cores of massive clusters at $z\sim0.2$–0.3.

In the light of this we address the recent claim by Wang & Ulmer (1997, hereafter WU) of a correlation between the blue fraction, f_{b}, and the ellipticity of the X-ray emission on large scales in a sample of clusters at $z\sim0.15$–0.6. We show the original data from WU in Fig. 11, where we also give similar observations of five clusters in our sample (those for which PSPC images are available). We have remeasured the ellipticities of the X-ray emission in all the clusters, both those in WU and the new clusters added here, inside a radius of 740 h^{-1} kpc, to confirm that our new measurements are on the same scale as the earlier values. We find a mean offset between the WU values and our measurements of $<\varepsilon-\varepsilon_{WU}>=-0.004\pm0.084$, with a typical deviation of $0.8\sigma_{WU}$ between the estimates. We conclude that our ellipticity measurements are in good agreement with those presented in WU and hence we can add our clusters to their

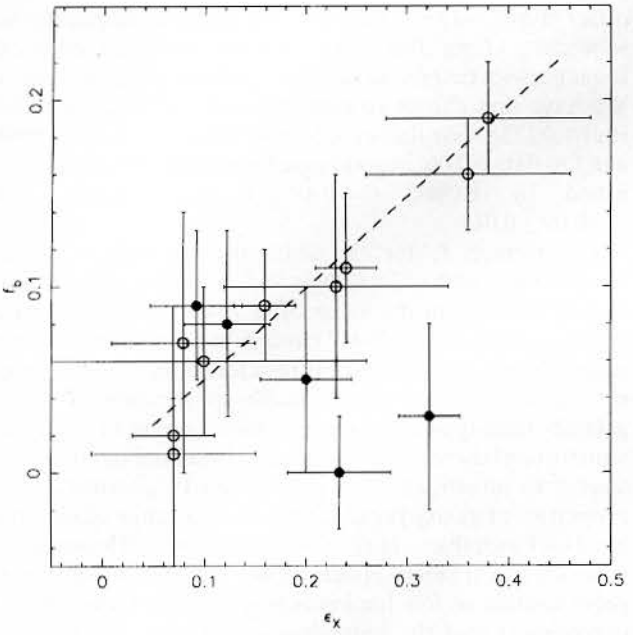

Figure 11. A plot of the blue fraction of the cluster population, f_b, versus the ellipticity of the X-ray emission of the cluster measured within a radius of $750\,h^{-1}$ kpc. The points marked as open symbols come from the analysis of Wang & Ulmer (1997) and the filled symbols are from this work (we have used our measurements for A1758). The dashed line is the best-fitting relation to the data from Wang & Ulmer (1997).

sample. The addition of our high-luminosity clusters to the already heterogeneous sample from WU obviously does not improve the correlation seen in their data (although neither does it completely destroy it). Moreover, we note that the presence of two points at high ε_X and high f_b appears to be responsible for much of the significance of their original correlation. One of these is the cluster A2125, which has an X-ray luminosity of only a tenth of the next lowest luminosity cluster in the sample, and as such is clearly a very different object from the remaining clusters in the figure. Removing this single object to provide a more homogeneous sample also removes any statistically significant correlation between f_b and ε_X. We therefore caution that the f_b–ε_X correlation reported by WU may simply be the result of a small and diverse sample. The lack of any correlation between f_b and ε_X for luminous X-ray clusters at $z \lesssim 0.3$ should not be surprising, given the generally low level of Butcher–Oemler activity in these clusters and their wide range of morphologies.

While our sample of clusters does lack a large population of luminous blue galaxies, looking at the values in Table 2 we can see that they do harbour a substantial population of star-forming galaxies, albeit at considerably fainter magnitudes than those used to trace the Butcher–Oemler effect. As we show below, the characteristic V-band luminosity of the blue populations in these clusters is considerably fainter than that of the cluster ellipticals, in contrast to the situation in more distant clusters at $z \sim 0.5$ where the blue spiral population have a characteristic luminosity brighter than that of the ellipticals (Smail et al. 1997a). This may be hinting at a redshift–luminosity relation for the active population in the clusters, with the characteristic luminosity of the star-forming class of galaxies increasing with redshift. A similar proposal has recently been made for the evolution of the star-forming population in the distant field (Lilly et al. 1995). Lilly et al. (1995) claim that the characteristic luminosity of the bluer field galaxies may brighten by up to a magnitude out to $z \sim 0.5$. Combining this evolution with the increased accretion rate on to massive clusters at moderate redshifts, it may be possible to explain the redshift evolution of the Butcher–Oemler effect using a simple infall model (Bower 1991).

We now look in more detail at the colour distribution within this faint blue cluster population to better understand its subsequent evolution. We address this using the two-dimensional distributions from Fig. 3 and project these on to the axis defined by the non-evolved SEDs seen in that figure. This allows us to crudely classify the various galaxy populations in terms of their equivalent present-day spectral type. We see a broad distribution of spectral classes, the frequency and breadth of this distribution is at odds with that seen at similar luminosities in comparably massive local clusters. Fitting to the luminosity distribution of the population with colours of an Sab or bluer in $(B-I)$, we find $I^* = 20.5 \pm 0.5$ and a steeply rising faint-end slope, $\alpha = -1.4 \pm 0.3$. Thus the characteristics luminosity of this population is $M_V \sim -17.5 + 5\log h$, about 2.5 mag fainter than the elliptical population. This is in contrast to more distant clusters where the spiral popultaion has a characteristic luminosity similar to that of the cluster ellipticals (Smail et al. 1997a). Furthermore, the bulk of this population have colours similar to present-day Sbc–Scd galaxies, with comparatively few being as blue as would be expected for vigorously star-forming Sdm galaxies. However, it should also be kept in mind that the absence of objects as blue as very late-type spirals from our clusters may be partly explained by the limiting magnitude of our sample ($M_V \gtrsim -16 + 5\log h$). With the advent of mid-UV surveys of local clusters (Brosch et al. 1997), it will become possible to trace the evolution of the UV luminosity function (and hence the mean star formation rate) in cluster environments from $z = 0$, and to compare this to the strong increase in star formation seen in the distant field, amounting to a factor of $\sim 2\times$ increase in the luminosity density at 2800 Å out to $z \sim 0.2$ (Lilly et al. 1996). Such a comparison would determine whether the mean star formation rates in clusters evolve in a manner similar to that in the surrounding field, or whether the cluster environment produces an additional long-term decline in the star formation rates of cluster galaxies at recent epochs.

If the cluster environment is producing a widespread decline in the star formation rates of member galaxies, we can ask how the clusters we see at $z \sim 0.24$ might appear today, in particular where the various galaxy populations we have identified would appear in the luminosity distribution of a local rich cluster. To do this we need to model the evolution in their star formation rates with time. This can only be done approximately, of course, given our lack of knowledge of their detailed dynamical history and previous star formation. Nevertheless, at this stage it suffices to determine what the simplest model for the star formation rate of the cluster population might predict at the present day. We start with the expectation that the star formation

rate in all cluster galaxies will decline towards the present, and hence for simplicity we have chosen to truncate the star formation in all the cluster galaxies at $z=0.24$ and evolve them forward to the present day, allowing the stellar population of the galaxies to fade and redden by the amount expected from the models. One attractive model for stopping star formation in cluster galaxies is to deplete their gas reservoirs by removing their haloes through interaction with the intracluster medium (Larson, Tinsley & Caldwell 1980). While other more drastic alternatives are possible, and may be necessary to form some of the more extreme spectral features observed in some cluster galaxies (Couch et al. 1994), this basic mechanism is sufficient to produce the drop in star formation required in our simple model. We will next assume that a galaxy with colours similar to a particular spectral type at $z=0.24$ would, if left undisturbed, retain that spectral type until the present day. This allows us to use the evolutionary models of Fioc & Rocca-Volmerange (1998), which fit the local spectral types (E-Sdm), to describe the star formation histories of the various galaxy populations in our clusters. We can then take these models and truncate the star formation at $z=0.24$ before evolving them to $z=0$. Using Fioc & Rocca-Volmerange's spectral synthesis code (PEGASE, Fioc & Rocca-Volmerange 1998) we can then determine the amount of fading and reddening the various spectral types would undergo, in their rest frame R and $(U-R)$ respectively. The evolution of the stellar populations, after the star formation (if any) is truncated, produces different degrees of subsequent reddening between $\Delta(U-R)=0.09$ for an elliptical to $\Delta(U-R)=0.77$ for an Sdm; the equivalent fading in the rest frame R is $\Delta R=0.30$ for an elliptical and $\Delta R=0.94$ for an Sdm.[5]

The predicted fading and reddening from our model should be viewed as the maximum allowed for a continuously star-forming galaxy; both are lower in the event that either the star formation was halted prior to $z=0.24$ and we are observing the already fading remnant, or the star formation continues to lower redshift before being truncated. However, the predicted fading and reddening can be exceeded if the star formation is burst-like, as appears to be necessary for modelling some of the spectral properties of distant cluster galaxies (e.g. Couch et al. 1998; see also Abrahams et al. 1996). More substantial fading of this population would also result if dynamical processes (stripping, harassment, etc.) removed stellar material from the galaxies. Moreover, we would expect different fading rates across this population in those scenarios in which the efficiency of removing material is a function of bulge strength (i.e. Hubble type), as appears to be the case for the harassment mechanism (Moore et al. 1996, 1997). Indeed, the harassment model predicts substantial stripping from later types (Sdm/Irr) and low-surface-brightness galaxies, possibly amounting to $\sim$90–95 per cent of their stellar material, while leaving early-type Sab galaxies relatively untouched (apart from the truncation of the star-formation in their discs). Thus it is conceivable that the strong-bulge, early-type spirals (Sab) would suffer only the fading expected from the stellar population model, whereas the later-type spirals would fade considerably more than our predictions, possibly up to 2–4 mag (Moore et al. 1997), because of the stripping of stars from these systems. Better predictions from the various theoretical models are required before we can make more detailed comparison.

To begin with, we ignore possible dynamical effects, and simply apply the evolution expected from our stellar models to the original distribution of galaxies in the cluster, as a function of their spectral type (Fig. 12). We show the results of this in Fig. 13, where we give both the original distribution at $z=0.24$ and that which would be observed for the same cluster at $z=0$. As can be seen in Fig. 13, the truncation of all the star formation in the clusters at $z=0.24$ results in a large population of faint, mid-type spiral galaxies moving towards the elliptical sequence. Concentrating on these fading spirals we would predict a characteristic magnitude of $M_V\sim -17+5\log h$ at the present day, and the population would retain the steep faint-end slope characteristic of the original blue cluster population ($\alpha=-1.4\pm0.3$). Adding the dynamically-driven, type-dependent fading discussed above would tend to produce two families of remnants. The stronger-bulged, and typically brighter, early-type spirals would end up around $M_V\sim -17+5\log h$, perhaps identifying them as precursors to the UV + group, while the bluer and later-type spirals would fade to $M_V\gtrsim -16+5\log h$, providing a natural source of the large population of dwarf elliptical (dE) galaxies seen at these

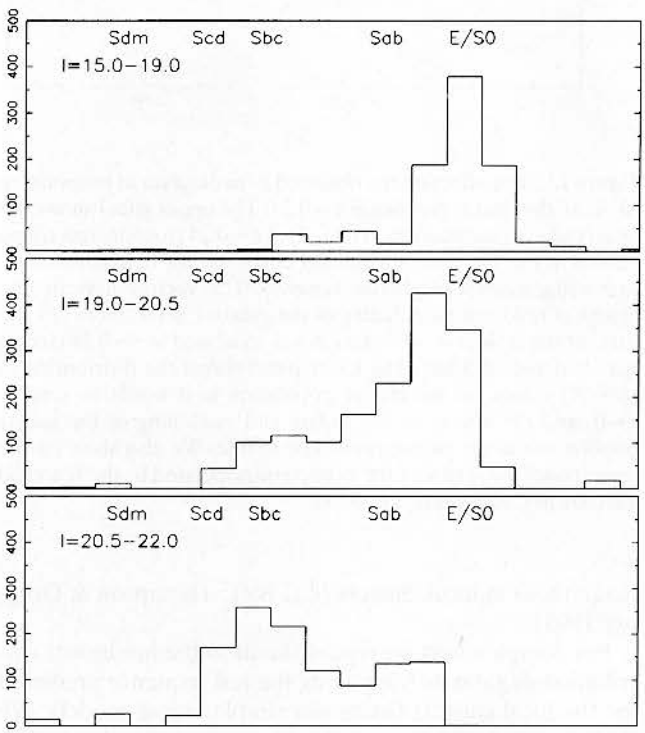

Figure 12. The combined distribution of galaxies from the 10 clusters, after field correction, projected along the axis defined by the colours of the non-evolved SEDs shown in Fig. 3. This is shown for each of the three independent magnitude slices, $I=15.0$–19.0, $I=19.0$–20.5 and $I=20.5$–22.0 in Fig. 3. We mark the equivalent spectral type for L^* galaxies across the tops of the figures. No correction has been made for the variation in elliptical colour with luminosity; this results in a gradual shift of the elliptical sequence to the left in the fainter samples.

[5]Here we assume a cosmology with $h=0.5$ and $\Omega=1$, giving a look-back time to $z=0.24$ of 4 Gyr.

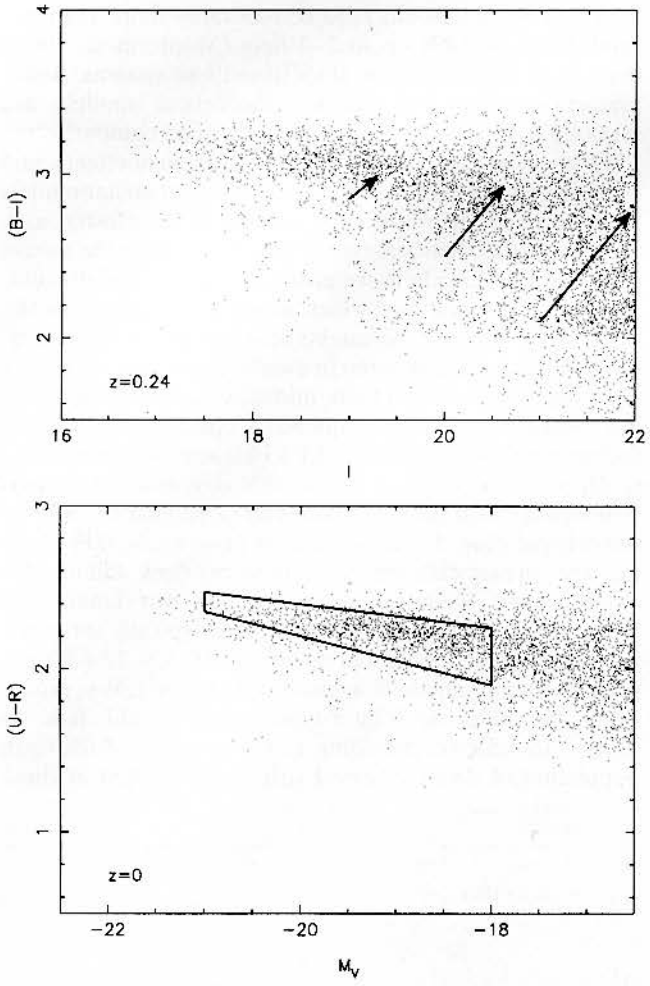

Figure 13. The effect on the observed c–m diagram of terminating SF in all the cluster galaxies at $z=0.24$. The upper panel shows the observed c–m distribution in $(B-I)$ at $z\sim0.24$ [roughly rest frame $(U-R)$]; this has been statistically corrected for field contamination using nearest-neighbour removal. The vectors indicate the extent of reddening and fading of the galaxies in our model by the present day if their star-formation was truncated at $z=0.24$ (for an Sab, Scd and an Sdm). The lower panel shows the distribution in $(U-R)$ colour for the cluster population as it would be seen at $z=0$, and the effects of the fading and reddening of the stellar populations in the galaxies is clearly visible. We also show on the lower panel the region of the c–m plane populated by the E and S0 galaxies in Coma studied in BLE.

magnitudes in local clusters (e.g. BST; Thompson & Gregory 1993).

For completeness we repeat the fit to the luminosity distribution of galaxies lying along the red sequence predicted for the local clusters (using our simple fading model). We find that the evolution of the blue population leads to a general steepening of the faint end of the distribution. Repeating the fit of a composite Gaussian + Schechter function to the luminosity distribution along the red sequence, we find that the faint-end slope is expected to steepen by $\Delta\alpha=-0.34$ from $\alpha\sim-1$ closer to $\alpha\sim-1.4$ as a result of the truncation of star-formation at $z=0.24$. Here we have evolved the parameters describing the brighter elliptical component to reflect the expected evolution to $z=0$. The resulting faint-end slope lies close to that seen in the coma cluster today, $\alpha=-1.4$ (Biviano et al. 1995). While our simple model has provided a possible outline of where the remnants of the galaxy populations identified in the distant clusters might be found today, we reiterate that much more detailed models, including information on both the dynamics and the previous evolutionary history of the galaxy populations, are needed to conclusively tackle this problem (cf. Baugh et al. 1996b).

4 DISCUSSION AND CONCLUSIONS

We have analysed the galaxy populations in the 10 luminous X-ray clusters in our sample on an individual cluster-by-cluster basis. The interest in this sample comes from its selection from the most massive clusters at $z\sim0.2$, allowing a simple comparison to the properties of the richest local clusters. Furthermore, using the uniformity of our sample and data set we have been able to combine the galaxy populations across all the clusters to provide a more detailed view of their typical populations. The galaxy mix in our clusters at bright magnitudes is characterized by a population of luminous red galaxies, with only a small fraction of blue, star-forming galaxies (~5 per cent) and an even smaller fraction of UV+ objects (~0.5 per cent). We find that the typical colours of the luminous ($M_V\leq-18.5+5\log h$) red galaxies are highly homogeneous across all the clusters in our sample. The intrinsic scatter in the typical colours of this population between clusters is $\lesssim2$ per cent in rest frame $(U-R)$. In our bluer colour, rest frame (2900-Å $-U$), the scatter may be larger but our photometric precision is not as high, leading to a limit on the cluster-to-cluster variation of $\lesssim5$ per cent in their mean colours. These observations thus extend the studies of BLE and Ellis et al. (1997) across a larger sample of clusters and into the mid-UV. We conclude that the brightest cluster galaxies comprise a homogeneous population longward of 2900 Å in their rest frame. We illustrate the type of constraints on cluster formation which this observation can provide using a very simple model. The model allows us to convert the observed cluster-to-cluster scatter in the mean colours of cluster ellipticals into a joint constraint on the lower limit of the formation epoch for this population and the maximum size of the structures in which they can coherently form. While the model we use is not physically well motivated, it does provide some insight into the information on cluster formation which these observations can provide. A rigorous theoretical analysis of the scatter expected in the colours of luminous ellipticals both within clusters (e.g. Ellis et al. 1997) and between clusters is urgently required.

A comparison between the integrated luminosity of the red cluster galaxies with the X-ray temperatures of seven of the clusters in our sample shows a good correlation between the two observables with a scatter of only ~17 per cent. We conclude that the total luminosity of the elliptical population in the clusters is a reasonable tracer of the cluster mass. Again, this is an interesting observation to tackle with theoretical models of cluster formation and growth, which can be robustly applied to our sample due to the well-defined cluster selection originally used.

The picture of widespread uniformity abruptly changes as we probe fainter in the clusters. Beyond

$M_V \geq -17.5 + 5\log h$, we start to detect an increasing population of blue cluster galaxies. These objects fall into two groups, galaxies blue in both $(U-B)$ and $(B-I)$ (about $\sim$30 per cent of the population) and those which, while having blue $(U-B)$ colours, are red in $(B-I)$: the latter are the UV+ galaxies, which comprise $\sim$5 per cent of the total cluster population and $\sim$50 per cent of the faint cluster population with red $(B-I)$ colours. The latter class of galaxies defines an extension of the narrow red sequence of the luminous ellipticals in the $(B-I)$ c–m plane. The same is not true in $(U-B)$ where they exhibit a substantial spread in colours, in contrast to the brighter ellipticals. The flux of a galaxy around 2900 Å, as probed by our $(U-B)$ colours, traces residual star formation (Dorman et al. 1995), being $\sim$50 per cent more sensitive to low levels of star formation than our $(B-I)$ colour for standard initial mass functions (IMFs). Thus the wide range in $(U-B)$ colours for this population indicates a spread in current star formation, albeit at a low enough level that it does not substantially perturb their red $(B-I)$ colours. The lack of a strong signature in the 4000-Å colours of these galaxies means they are not included in the standard Butcher–Oemler definition for the blue fraction of the cluster population, although neither are they completely passive.

The fates of these two blue populations in present-day clusters are of considerable interest. We propose that, in the absence of dynamical processes or a reactivation of star formation, the UV+ population will undergo only modest fading in optical luminosities from that observed at $z \sim 0.24$. As the clusters we study are amongst the most massive formed at their epoch, we assume that the galaxy populations of these clusters should evolve to be similar to that seen in the richest local clusters. Therefore, these galaxies should contribute a large proportion of the quiescent, red $M_V \sim -17.4 + 5\log h$ population in the most massive local clusters ($M \geq M_{\rm Coma}$). Of the $I \geq 20.5$ galaxies in the distant clusters with red $(B-I)$ colours, roughly 50 per cent lie in a blue tail in $(U-B)$. The high proportion of such objects indicates that a large fraction of the quiescent $M_V \sim -17.4 + 5\log h$ population in local clusters must have passed through this stage. The morphological mix in the Coma cluster at these magnitudes is dominated by S0 galaxies, which make up 65 per cent of the population, with ellipticals making up 30 per cent and Sa galaxies most of the remaining 5 per cent (Dressler 1980). Thus while some of the UV+ galaxies may continue to form stars at a low level and hence appear as Sa galaxies in the local clusters, the majority must be precursors to the S0 or E populations. Moreover, the typical magnitude of these galaxies corresponds to a luminosity close to the characteristic value for the S0 populations in local clusters. BST claim a mean luminosity of $< M_V > \sim -17.3 + 5\log h$ for the S0 galaxies in Virgo [assuming $(B-V) \sim 0.6$], while Thompson & Gregory (1993) find $< M_V > \sim -17.8 + 5\log h$ for the S0 population of Coma. In the light of this and the observations of a rapid decline in the numbers of S0 galaxies in $z \geq 0.4$ clusters (Dressler et al. 1998), we suggest that the faint galaxies observed in our $z \sim 0.2$–0.3 clusters with red $(B-I)$ colours, but blue $(U-B)$, may be the precursors of today's S0 cluster population, the characteristics of which they would closely match (cf. Abrahams et al. 1996).

By morphologically classifying a small number of the $I \geq 20.5$ Red and UV+ population using WFPC-2 imaging of A2390 we demonstrate that the faint, red cluster population does consist of spheroidal galaxies and we also show marginal evidence that the S0 component of this population may exhibit a wider range, and typically bluer, mid-UV colours than the faint ellipticals. The substantial deficit of S0s in clusters at $z \sim 0.5$ (Dressler et al. 1998), along with our suggested identification of the UV+ population with the precursors of the S0 population of local rich clusters, would indicate that $z \sim 0$ S0s should show some signs of their recent transformation. The spectral signatures of recent star formation have been seen in samples of spheroidal galaxies from the Coma cluster (Caldwell et al. 1993), although these have not been linked specifically to the S0 population. Moreover, in a comparison of the dispersions in the $(U-V)$ colours of luminous ellipticals and S0s in Coma, BLE concluded that both populations showed essentially no intrinsic scatter. Clearly issues of luminosity and morphology must be addressed before we can fully understand the evolution of the galaxy populations of clusters. Central to this understanding will be further work on classifying samples of faint galaxies in $z \sim 0.1$–0.3 clusters; these will enable us to robustly track the morphological evolution of this population (Couch et al. 1998).

The fate of the blue star-forming galaxies in these distant clusters is more speculative. These are typically low-luminosity systems ($L_V \sim 0.001 L^*$), exhibiting relatively modest star formation. We illustrate one possible evolutionary pathway, which the population would follow if its star formation was terminated at $z = 0.24$; this produces a population of faint red galaxies in local clusters with a steep luminosity distribution. These characteristics are similar to those of the dwarf elliptical population which dominates local clusters at faint magnitudes (BST). Recent spectroscopic observations of similar objects in a cluster at $z = 0.4$ has shown them to have very low masses (Koo et al. 1997), so we caution that these low-luminosity galaxies may be quite fragile and hence the cluster environment could have a significant impact on their luminosity and morphological evolution through dynamical processes (Moore et al. 1996). If substantial amounts of baryonic material are removed from late-type galaxies during their accretion on to the clusters, we would expect this material to be deposited into the cluster potential as either intracluster gas or intracluster light. Tracing the evolution of these components within rich clusters at $z \sim 0$–0.5 may provide the most direct test of the stripping and harassment mechanisms (Moore et al. 1998).

In conclusion, there is a growing body of evidence which indicates that the passive red galaxy populations in local clusters are produced by a diverse range of processes. The most luminous elliptical galaxies appear to have formed at very early epochs ($z \gtrsim 3$; Ellis et al. 1997; Stanford et al. 1998), while the bulk of the S0 population have come into being much more recently ($z \lesssim 0.5$, Dressler et al. 1998), as may the lower luminosity dwarf ellipticals (Koo et al. 1997). By combining the galaxy samples from our uniform survey of clusters, we have identified a class of galaxies in our distant clusters which would have characteristics similar to those of the S0 population at low redshift, but which still show residual traces of star formation, consistent with the

S0 population having previously been more active. Determining the morphologies of a large sample of these objects in intermediate redshift clusters using *HST* will provide a strong test of their relationship to both the Butcher–Oemler populations of distant clusters and to the local S0s (cf. Larson et al. 1980).

ACKNOWLEDGMENTS

We would like to thank Steve Allen, Harald Ebeling, Andy Fabian and Hans Böhringer for their work in defining the X-ray sample on which our study is based. We also thank Jim McCarthy and Jim Westphal for their work in providing an efficient UV imaging capability on the 5-m, essential for our observations, as well as Jim Schombert for kindly loaning us his *U* filter, David Hogg for providing his deep *U*-field exposure, Alan Dressler for donating 5-m time to undertake the *BI* imaging of the same field and David Buote for the analysis of the shapes of the cluster X-ray emission used in Fig. 11. We thank the referee, Phil James, for his thorough reading of the paper and constructive comments which improved the text, particularly in regard to the discussion of the models. Finally, we thank Rebecca Bernstein, Richard Bower, Julianne Dalcanton and Roger Davies for extensive discussions on the nature and evolution of cluster galaxies. IRS acknowledges support from a PPARC Advanced Fellowship and ACE from a Royal Society Fellowship. RDB acknowledges NSF grants AST 92-23370 and AST 95-29170. The research published here used the STARLINK computer resources at the University of Durham. This work is based on observations obtained at Palomar Observatory, which is owned and operated by the California Institute of Technology.

REFERENCES

Abrahams R. G. et al., 1996, ApJ, 471, 694
Allen S. W., 1995, MNRAS, 276, 947
Allen S. W. et al., 1996, MNRAS, 283, 263
Aragón-Salamanca A., Ellis R. S., Couch W. J., Carter D., 1993, MNRAS, 262, 764
Barger A. J., Aragón-Salamanca A., Ellis R. S., Couch W. J., Smail I., Sharples R. M., 1996, MNRAS, 279, 1
Barger A. et al., 1998, ApJ, submitted
Baugh C. M., Cole S., Frenk C. S., 1996a, MNRAS, 282, 27
Baugh C. M., Cole S., Frenk C. S., 1996b, MNRAS, 283, 1361
Belloni P., Bruzual A. G., Thimm G. J., Roser H.-J., 1995, A&A, 297, 61
Bertin E., Arnouts S., 1996, A&AS, 117, 393
Bessell M., 1990, PASP, 102, 1181
Binggeli B., Sandage A., Tammann G. A., 1985, AJ, 90, 1681 (BST)
Biviano A., Durret F., Gerbal D., Le Fèvre O., Lobo C., Mazure A., Sleazak E., 1995, A&A, 297, 610
Bower R. G., 1991, MNRAS, 248, 332
Bower R. G., Lucey J. R., Ellis R. S., 1992, MNRAS, 254, 601 (BLE)
Broadhurst T., Villumsen J. V., Smail I., Charlot S., 1997, ApJ, submitted
Brosch N., Formiggini L., Almoznino E., Sasseen T., Lampton M., Bowyer S., 1997, ApJS, 111, 143
Butcher H., Oemler A., 1978, ApJ, 226, 559
Butcher H., Oemler A., 1984, ApJ, 285, 426 (BO84)
Byrd G., Valtonen G., 1990, ApJ, 350, 89
Caldwell N., Rose J. A., Sharples R. M., Ellis R. S., Bower R. G., 1993, AJ, 106, 473
Colless M. M., 1989, MNRAS, 237, 799
Couch W. J., Sharples R. M., 1987, MNRAS, 229, 423
Couch W. J., Ellis R. S., Sharples R. M., Smail I., 1994, ApJ, 430, 121
Couch W. J., Barger A. J., Smail I., Ellis R. S., Sharples R. M., 1998, ApJ, in press
Dorman B., O'Connell R. W., Rood R. T., 1995, ApJ, 442, 105
Dressler A., 1980, ApJS, 42, 565
Dressler A., Gunn J. E., 1992, ApJS, 78, 1
Dressler A., Oemler A., Butcher H., Gunn J. E., 1994, ApJ, 430, 107
Dressler A., Oemler A., Couch W. J., Smail I., Ellis R. S., Barger A., Poggianti B. M., Sharples R. M., 1998, ApJ, in press
Ebeling H., Voges W., Bohringer H., Edge A. C., Huchra J. P., Briel U. G., 1996, MNRAS, 281, 799
Edge A. C., Stewart G. C., 1991, MNRAS, 252, 428
Edge A. C., Smail I., Ellis R. S., Blandford R. D., Ebeling H., Allen S. W., Fabian A. C., Kneib J.-P., 1998, MNRAS, submitted
Ellis R. S., Smail I., Dressler A., Couch W. J., Oemler A., Butcher H., Sharples R. M., 1997, ApJ, 483, 582
Faber S. et al., 1997, preprint
Fusco-Femiano R., Hughes J. P., 1994, ApJ, 429, 545
Fioc M., Rocca-Volmerange B., 1998, A&A, in press
Gunn J. E., Gott J. R., 1972, ApJ, 176, 1
Hogg D. W., Pahre M. A., McCarthy J. K., Cohen J. G., Blandford R. D., Smail I., Soifer B. T., 1997, MNRAS, 288, 404
Kodama T., Arimoto N., 1997, A&A, 320, 41
Koo D. C., Guzmán R., Gallego J., Wirth G. D., 1997, ApJ, 478, L49
Landolt A. U., 1992, AJ, 104, 340
Larson R. B., Tinsley B. M., Caldwell C. N., 1980, ApJ, 237, 692
Lea S. M., Henry J. P., 1988, ApJ, 332, 81
Lilly S., Tresse L., Hammer F., Crampton D., Le Fèvre O., 1995, ApJ, 455, 96
Lilly S., Le Fèvre O., Hammer F., Crampton D., 1996, ApJ, 460, 1
Moore B., Katz N., Lake G., Dressler A., Oemler A., 1996, Nat, 379, 613
Moore B., Lake G., Katz N., 1998, ApJ, submitted (astro-ph/9701211)
Mushotzky R. F., Scharf C. A., 1997, ApJ, 482, L13
Pierre M., Le Borgne J. F., Soucail G., Kneib J.-P., 1996, A&A, 311, 413
Smail I., Hogg D. W., Yan L., Cohen J. L., 1995a, ApJ, 449, L105
Smail I., Hogg D. W., Blandford R. D., Cohen J. G., Edge A. C., Djorgovski S. G., 1995b, MNRAS, 277, 1
Smail I., Dressler A., Couch W. J., Ellis R. S., Oemler A., Butcher H., Sharples R. M., 1997a, ApJS, 110, 213
Smail I., Ellis R. S., Dressler A., Couch W. J., Oemler A., Butcher H., Sharples R. M., 1997b, ApJ, 479, 70
Stanford S. A., Eisenhardt P. R., Dickinson M. E., 1998, ApJ, in press
Thompson L. A., Gregory S. A., 1993, AJ, 106, 2197
van Dokkum P. G., Franx M., 1996, MNRAS, 281, 985
Wang Q. D., Ulmer M. P., 1997, preprint (astro-ph/9702069) (WU)
Wilson G., Smail I., Ellis R. S., Couch W. J., 1997, MNRAS, 284, 915
Zabludoff A. I., Zaritsky D., Huan L., Tucker D., Hashimoto Y., Shectman S. A., Oemler A., Kirshner R. P., 1996, ApJ, 466, 104